Chapter 2 Satellite image analysis

The satellite image analysis was made with LANDSAT TM images. In the first fiscal year, photogeologic diagnosis and interpretation of thirteen scenes covering the whole survey area were conducted using false color images and ratio images. In the second fiscal year, precise analysis of alteration zones with iso-grain model was tried for six scenes including promising districts narrowed from the first fiscal year (phase 1) survey. In the following section the summary is described of analyses using false color and ratio images of LANDSAT TM in the first fiscal year (phase 1). For details, readers refer to page 56 to 214 of the first fiscal year report (JICA/MMAJ, 2000).

2-1 Analysis of false color image and ratio image

2-1-1 Data used

For use in the geological and tectonic analysis and alteration zone extraction of this area, 13 scenes of false color and ratio images were prepared. In addition, a false color digital mosaic image and a ratio mosaic image covering the whole area were prepared. Most of the data were observed by LANDSAT 5 (by LANDSAT 4 for a scene of Path 231/Row 91) and bulk-corrected CCT's (computer-compatible magnetic tapes) that were purchased from the EROS Data Center of the U.S. Geological Survey through the Remote Sensing Technology Center. The position of images of the 13 scenes is shown in Fig. II-2-1, and the date of observation and the information on the sun position is given in Table II-2-1.

In purchasing the data, the LANDSAT TM data available at the U.S. EROS Data Center covering the survey area was first inquired through the Remote Sensing Technology Center. The best choice for image analysis was selected in consideration of data deficiency, the amount of cloud and snow, and the time of observation. Further, for the naming of each scene of the image, a name of a representative city or town of the area in the image was employed. Serial numbers were given from the northwestern end to the southeastern end.

In the preparation of false color images and ratio images a method was developed by which the same lithofacies and the same alteration zones can be expressed in the same color tone, even though scenes to which they belong are different. Also, with the same band combination with false color images, a 13-scene digital mosaic image covering the whole area was produced. When making a mosaic image, attention was paid to avoiding different color tones between adjacent images. The methods of image preparation are respectively discussed below.

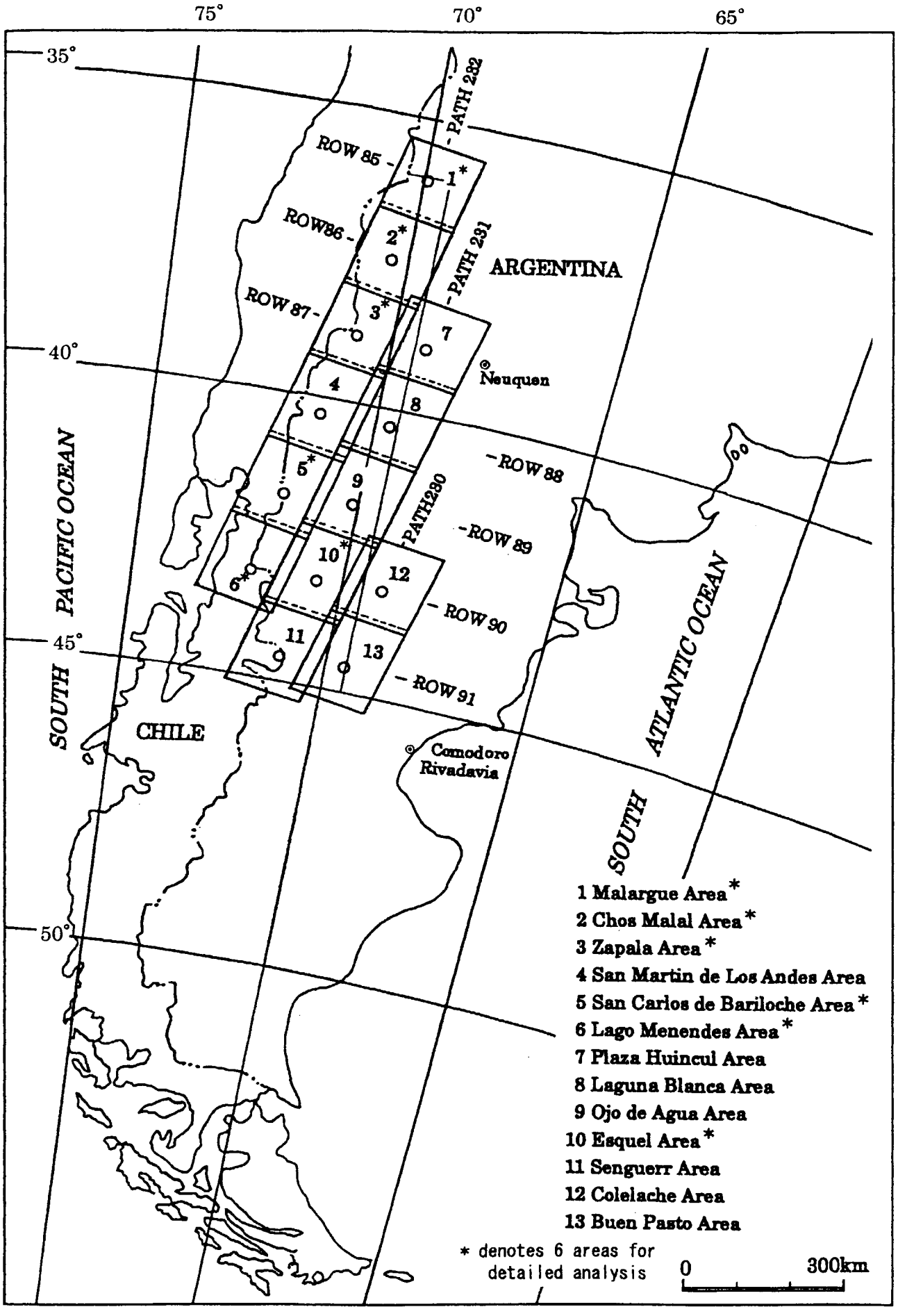

Fig. II-2-1 Index map of 13 scenes of Landsat TM image over the survey area

Table II-2-1 Path/Row, date of acquisition, sun azimuth and sun elevation of 13 scenes of the LANDSAT TM image.

No.	Name of the scene (area)	Path	Row	Date of acquisition	Sun azimuth	Sun elevation
1	Malargue	232	85	Feb. 9, 1987	75°	44°
2	Chos Malal	232	86	Feb. 9, 1987	74°	44°
3	Zapala	232	87	Feb. 9, 1987	73°	43°
4	San Martin de Los Andes	232	88	Feb. 9, 1987	72°	42°
5	San Carlos de Bariloche	232	89	Feb. 22, 1986	65°	40°
6	Lago Menendez	232	90	Dec. 7, 1986	73°	50°
7	Plaza Huincul	231	87	Jan. 1, 1987	80°	50°
8	Laguna Blanca	231	88	Oct. 29, 1986	63°	46°
9	Ojo de Agua	231	89	Oct. 29, 1986	62°	45°
10	Esquel	231	90	Jan. 27, 1985	71°	46°
11	Senguerr	231	91	Feb. 24, 1992	68°	34°
12	Colelache	230	90	Dec. 9, 1986	73°	50°
13	Buen Pasto	230	91	Dec. 9, 1986	72°	49°

2-1-2 Image processing and preparation method

1) Preparation of the false color image

a) Radiant quantity correction

In order to prepare the false color image, correction of radiant quantity is required, which includes quantity correction of incident light, atmospheric correction and correction of directional reflection. Spectral ranges of a sensor called TM (Thematic Mapper) on board the LANDSAT are four bands in the visible to near-infrared range, two bands in a short-wave-infrared range and one band in a thermal-infrared range, totaling seven bands in all. The observed analog image data are converted into 256 gradations of digital values from 0 to 255 per pixel.

The luminance obtained by an optical sensor such as LANDSAT TM reflects sunlight from the earth surface in the visible to near-infrared range and thus makes it possible to discern surface objects by the difference of spectral reflectance inherent to such objects. The spectral radiance incoming to the satellite sensor passes through the atmospheric layers while the sunlight is reflected on the earth surface and reaches the satellite. Thus, the radiance reaching the satellite sensor includes, in addition to reflected light from the earth, radiation light from the atmosphere, scattered light and scattered radiation (sky light) that is incident in all directions after scattering of sunlight (path radiance) in the atmosphere. The spectral radiance as obtained by the sensor observing just the underneath at a wavelength of λ can be approximated by the following equation:

$$L(\lambda_1, \lambda_2) = \int_{\lambda_2}^{\lambda_1} K(\lambda)[\tau a(\lambda)\{U(\lambda) + P(\lambda)\}\rho(\lambda) + b(\lambda)]d\lambda \qquad ①$$

$L(\lambda_1, \lambda_2)$	: spectral radiance from wavelength λ_1 to λ_2 entering the sensor
$K(\lambda)$	: system response of the sensor
$\tau a(\lambda)$	: atmospheric transmittance of reflected light
$U(\lambda)$	: radiance of direct sun light
$\rho(\lambda)$	: reflectance of the ground (earth surface)
$b(\lambda)$	: atmospheric radiation and scattered light between the sensor and the object
$P(\lambda)$	: radiance of sky light ? (downward scattered sun light)

Because the effect of these elements is different depending on quantities of steam and aerosol in the atmosphere, the same value is not obtained on the same material if an observation is made at a different time. Also, the effect of these absorbed light and scattered light is dependent on the wavelength, so that the band ratio of spectral reflectance of a material does not have a fixed value in images acquired at different times. Consequently, if images are processed with the radiant quantities of each band being uncorrected, the same material is expressed in different color tones, thereby making the comparison and discrimination of materials impossible.

Because the image data used for this analysis were acquired on many occasions, the correction of radiant quantities was made on the basis of the following assumptions in order to express the same material in the same color tone in all of the images:

- System response of the sensor is an output in a first-order linear form (i.e., y = ax) to the incident luminance.
- The atmospheric transmittance of reflected light is equal at any portion within an image.
- The atmospheric radiation and scattering between the sensor and the object are equal at any portion within an image.
- The sky light radiance is equal at any portion within an image.

(i) Correction of quantity of incident light

The radiance of direct sun light which is incident on a unit area differs from location to location even within an image. Hence, the incident light is corrected so that the sun elevation is fixed at 60° from the geographical coordinate of each pixel, the sun azimuth and the sun elevation which were given to the image.

(ii) Atmospheric correction

Atmospheric correction is conducted to correct the atmosperic transmittance for reflected light, $\tau a(\lambda)$, and atmospheric radiation and scattered light between the sensor and the object, $b(\lambda)$. This correction requires the values of incident light quantity, $\{U(\lambda) + P(\lambda)\}$, and surface reflectance, $\rho(\lambda)$.

The correction of quantity of incident light presupposes that all the objects within an image are flat. In reality, however, there are terrane undulations, which give different values of $\{U(\lambda) + P(\lambda)\}$ for the same location in two images acquired at different times because of a difference in solar position. The use of a high-precision DTM (digital terrane model) to correct the value of $\{U(\lambda) + P(\lambda)\}$ may be one solution of this problem. This solution, however, does not seem realistic because areas to which a high-precision DTM can be applied are limited. Consequently, a method was employed to use numerous pixels corresponding between two images and to statistically process the overlaps to eliminate dependency on terrane undulations.

As the atmospheric correction between observations on a day has higher precision, the atmospheric correction of all the thirteen scenes was conducted with the following procedures:

(a) Atmospheric correction was made for each path. The northern end scene of each path was taken as a reference image.
(b) Atmospheric correction of each image was proceeded southward one by one.
(c) The central path (P231) was taken as a reference for the atmospheric correction among the three paths.

By undergoing these processes, it is possible to make the atmospheric condition over the entire image agree with that over a scene of the central north end image (P231/R087).

(iii) Correction of directional reflection coefficient

In a perfect diffusion reflective material, suppose that the reflective coefficient of reflected light is 1 that is vertically incident on the material and is vertically observed. If the observation position is changed from vertical to horizontal, the reflective coefficient will gradually decrease from 1 to 0.

Each image of LANDSAT TM has a transverse (roughly E-W direction) angle of visibility of *ca.* 16°. This results in an angular difference of *ca.* 16° between the right and left sides of an image for the angle formed by the sun, the observed material and the observer when the sunlight radiates from the right side of an image. In such a case, the same phenomenon will

occur as observing a perfect diffusion reflective material from a different angle. Because the directional reflection coefficient varies with materials and wavelengths and is dependent on topography, it is impossible to correct it for each pixel. If the east end and the west end of the image are compared within an image (on the assumption that the sun radiates from the east at 90° azimuth and 60° elevation, that there are no undulations on the surface, and that the same material as basalt of the moon is distributed), however, luminance is reduced by about 10% on the right (east) side where an angle formed by the sun, the object and the observer becomes larger. When three images are joined from east to west, this causes luminance difference between the east end and west end images. For example, if the luminance is 1 for the west end image, that of the east end image will become about 27% less ($=0.9^3$), making the east end image obviously darker.

This necessitated examination of how luminance was changing over the entirety image. It was executed by the use of statistics based on the atmospherically corrected images. In the analysis carried out so far in "the eastern Andean area of the Argentine Republic", luminance reduction of about 7% was observed in the eastern side of a scene. This analysis, by applying this factor and compensating the reduced luminance by about 7% per scene, could obtain a generally flat average luminance curve except for both the left end of the image (areas with snow and sea) and the right end where sufficient data were not available.

b) Luminance correction and filter processing

By means of the above radiation quantity correction method, the luminance of all the scenes were unified to the reference luminance of P231/R087. The statistics (average, standard deviation and distortion) of LANDSAT TM image data is different for each band, and the variance is generally small in a range of 20 to 30 (of 256 gradations). Consequently, if such data is used itself, the images will have unacceptable color balance, small variance, and small difference in color tone, and therefore will not be adequate for the interpretation of the image.

In order to solve these problems so that the radiation quantity correction over all the scenes of image can be appropriately produced, the same luminance correction was conducted for all the scenes using non-linear stretching. The method used for this work was non-linear stretching to attain a distribution close to the normal distribution having an average luminance of about 115 (256 gradations). Meanwhile, the normal distribution was calculated so that 2.5 times of the standard deviation would correspond to 115 gradations. The statistics of the entire area were calculated after removing areas with cloud, snow and water.

For enhancing the image, there are various methods including the Laplacian and Gaussian filters and local enhancement processes. The Gaussian filters and local enhancement processes, however, employ stretching methods variant from field to field to

emphasize difference from the surrounding materials. As a result even the same material could be shown in different color tone, if it is placed in a different field. Hence, the present image enhancement process employed only the Laplacian filters to avoid such an effect.

For the color combination of false color image, combinations of bands 1,4 and 5 (to blue, green and red), bands 1,4 and 7, and bands 4, 5 and 7 were examined. The survey area has a wide occurrence of intermediate volcanic rocks, and the combination of bands 1,4 and 5 is suitable to interpret the tectonics of intermediate volcanic rocks. Therefore, an image was created with the color combination of bands 1, 4 and 5 to blue (B), green (G) and red (R) respectively.

c) Geometric correction

The images were converted geometrically into the UTM coordinate using the prepared false color images and topographic maps (scale: 1/500,000). The most precise topographical map which was available for the analysis was in such a small scale as 1/500,000, and the greater part of the survey area consisted of mountains and deserts where no markers such as rivers were located. Therefore it was difficult to select high-precision GCPs (Ground Control Points). Then, river junctions and road crossings were used as GCPs and 15 to 20 points were selected per image. Pseudo Affine transform was used for interpolation and low-precision GCPs were deleted so that the error from the result of the least square method should be not more than 30 pixels (about 1 km).

The error with not more than 30 pixels corresponds to about 2 mm in a 1/500,000 scale topographical map, which is close to the limit of geometric correction when the precision of the topographic map and the conditions of survey area are taken into consideration. It should be noted that bi-linear interpolation was used for geometric conversion and re-sampling was carried out with a size of pixel being 30 m.

2) Preparation of the color composite ratio image

a) Principle of calculating ratio between bands

LANDSAT TM observes spectral radiance input to the sensor in the seven wavelength bands of visible to near-infrared and of intermediate-infrared. The radiance of an earth material as observed by the sensor, N_i (unit: mW/cm^2Sr), can be expressed by the following equation:

$$N_i=(1/\pi)(H_iR_iT_iA_i)+N_{pi} \qquad ②$$

H : radiance of sun-light

R : reflectance of the object on the surface

T : atmospheric trasmittance (vertical direction)

A : Coefficient determined by the following two angles

angle 1: between a line connecting sun and the surface object and the surface plane

angle 2: between the surface object and the sensor

N_p : Path radiance of the atmosphere

I : Band of the sensor

Because, if N_p is assumed, A becomes constant regardless of the channel, and H and T take fixed values by each channel , the spectral characteristics can be emphasized by the ratio between two channels (bands). This means that when looking into the ratio between channels of maximum and minimum values in a reflectance spectral of mineral, the ratio of a pixel which contains the mineral becomes larger and it is easy to discriminate it from other pixels which do not contain the mineral.

The basic idea of ratio image is to apply this characteristic to presenting the distribution of a certain mineral in the image.

The ratio image processing places the minimum digital value as the atmospheric path radiance, obtains the value by deducting the minimum value from the digital value of each band and obtains the ratio between these bands. The ratio between the bands is usually in a range of 0 to 10, but density conversion described in the last section (2-1-2 1 Preparation of the false color image) is necessary to express the ratio between bands in the image. The density conversion was conducted by the following procedure:

Referring to the known geological alteration zones recorded in the existing geological data, the distribution of ratio values was obtained for the alteration zones. The scope slightly larger than this distribution range was defined, and pixels having ratio value outside this scope were given the value of 0. Excepting ratio value of 0, the variance of the rest of ratio image processing values was smaller than the variance of the original ratio image processing values. Thus, the density conversion made the presentation possible in a variety of densities.

b) Examination of the ratio between the two bands

Porphyry copper deposits and epithermal gold deposits are distributed in the survey area, accompanied by the inherent hydrothermal alteration zones. The validity of the ratio between two bands (5/7, 4/5 and 3/1) for extracting of these hydrothermal alteration zones from the LANDSAT TM data was verified by the previous work in the Escondida area and the Belgua Progreso area, Chile.

In the present survey, in two areas of P232/R085 and P232/R086 where known alteration zones are present, the ratio images were compared by the combination of the ratio between

two bands (5/7, 4/5 and 3/1 for one, and 5/7, 4/7 and 4/5 for the other). As a result, it was found that the most effective for extracting alteration zones was the combination of 3/1, 4/5 and 5/7 allocated to blue (B), green (G) and red (R). In this combination, the alteration zones are shown in reddish pink and whitish pink colors. In the ratio image processing of other areas, the average of gain and bias that became the best in these two areas was used.

c) Analysis of principal components

From its nature, the ratio image makes it possible to eliminate shadows caused by topography. On the other hand, the loss of topographic features makes the area identification difficult. Hence, to make the area identification easier, the present survey added topographic information to the ratio to create images.

Two methods are available to express topographic features; one is the use of band 5 which reflects topographic features, and the other is the use of the first primary component in the analysis of main components which reflects topographic information. In this survey, the first primary component in the analysis of principal components was used.

For geometric correction, the same GCP as used for the geometric correction in the preparation of false color synthetic image was used, and geometric conversion to the UTM coordinate system was made by the same method.

3) Preparation of mosaic images

a) Image compression and geometric conversion

In order to create a 13-scene false color mosaic image which cover the entire areas, image compression was conducted to reduce the image size. If there was no image compression, the image produced after the creation of mosaics would be voluminous, comprising 17,000 pixels x 41,000 pixels x 6 bands = 4.2 GB, and the quantities of data would exceed the physical limit of film output.

From the image of each scene in which the radiant quantity was corrected, compression was made by the geometric conversion of bi-linear interpolation, and 16 pixels (4 x 4) were reduced to one pixel. Then, from the overlapping area of two images 10 to 20 corresponding points were visually selected and the geometric conversion coefficient was calculated by Helmert's conversion using the least square method. In this process, the coefficient of Helmert's conversion was obtained by eliminating data with large errors so that errors after re-calculation shall be not more than one pixel. Geometric conversion was executed by the use of bi-linear interpolation.

b) Stitching images

Images acquired at different occasions have areas of apparently different color tones in the joined area between two images attributable to changes in surface covers and the position of shadows and clouds. Even though this apparent change in color tone does not interfere geological interpretation, it will give an unsatisfactory impression to the completion of mosaic images. To improve this insufficiency, a "staggering image stitching method" was newly developed in which areas of smaller tonal difference were searched, and applied to join the images. In this method, areas that have clouds or in which shadow positions change can be detoured for joining.

Images were joined one by one starting from the northernmost image of each path, and three oblong mosaic images of P232/R085 to R090, P231/R087 to R091 and P230/R090 to R091 were made. Then, with the P231 mosaic image as a reference, the corresponding points on the image on either side of east and west were chosen. The images were joined by the above method after geometric conversion named Helmert's conversion. The image made by joining three paths was sized about 4,400 pixels x 10,200 pixels.

c) Geometric conversion

The mosaic image is long and narrow from north to south at Long. 68° W to 73° W and Lat. 35°30' S to 45°15' S. Therefore, map projection was made by using the UTM projection method which shows little distortion in the N-S direction. The central longitudinal line used was Zone 19 in which W69 is in the center. The spheroidal zone used was International 1909. Re-sampling was made by bi-linear interpolation and geometric conversion performed with 120 m/pixel.

2-1-3 Result of interpretation of satellite image analysis

1) Method of analysis

The purpose of this analysis is to make a photo-geological interpretation of the LANDSAT TM image and to analyze it with the existing data on geology, ore deposits and exploration data of the area. Through comprehensive examination of these information promising districts are selected.

The area covered by the analysis develops extensively from Lat. 35° S to 45° S along the border with Chile as shown in Fig. II-2-1. The area is covered by thirteen scenes of LANDSAT TM image and has a size of about 250,000 km^2.

The photo-geological interpretation of the satellite image usually comprises the following five steps:

(1) Preparation (Satellite data acquisition and orientation, collection and review of the existing geological and ore deposit data)
(2) Image processing and preparation
(3) Photo-geological and comprehensive interpretation (preparation of comprehensive interpretation map: comparison with the existing data)
(4) Field check survey and re-interpretation based on it.
(5) Report preparation

Of the above five steps, field check survey, (4), has been partly executed for the ground truth survey, but re-interpretation based on it has been made from the present analysis.

The criteria of the interpretation and their expression in the photo geology are as follows:

(A) Photo-characteristics
- Color tone: white, white gray, gray, blue gray, green gray, green, dark green, purple gray and brown, etc.
- Texture: fine grain, medium grain, coarse grain, smooth, etc.

(B) Morphological expression
- Drainage pattern: dendritic, parallel, latticed, plumous, etc.
- Drainage density: extremely low, low, moderate, high, extremely high.
- Rock resistance: extremely low, low, moderate, high, extremely high.
- Cross section: sloping geometry.
- Development of bedding: well developed, partially developed, massive, etc.

(C) Superficial cover
- Vegetation: dense, moderate, sparse.
- Cultivation: dense, moderate, sparse.

The lineaments interpreted and extracted from the satellite image reflect the earth surface or shallow underground fractures and, in the photo-geological method, are generally based on the recognition of the following topographical features:

(a) Presence of fault scarps.
(b) Presence of linear and wide fault valleys.
(c) Cases where river watercourses show significant linearity.
(d) Presence of kerncol and kernbut.
(e) Cases where the inclination change points on mountainside slopes continue linearly.
(f) Cases where moderately sloping sedimentary rock slopes suddenly turn to steep slopes in

linear succession.

(g) Cases of deviations in mountain ridges and river watercourses.

(h) Drainage anomaly (such as cases where latticed primary water streams are arranged linearly or the case of angular drainage system.

(i) Cases where lakes, hot springs, craters, springs and disintegrations are positioned in alignment.

(j) Cases of deviations in alluvial fan.

(k) Cases where river terraces (usually flat) have vertical gaps or horizontal deviations with a linear boundary.

The topographical feature making the key for the above judgement have local characteristics depending on the rocks, tectonics or geological age of the areas in question; therefore, the degree of their appearance is variable from area to area. In the covered area, the topographies of (a), (b), (c) and (e) were conspicuous and those of (f), (g), (h) and (i) were also observed in part. In the meantime, to interpret the topographies of (i), (j) and (k), it would be necessary to use larger-scale image scenes or to see the spot HRV image scene and aerial photographs three-dimensionally.

2) Result of analysis

a) Result of 13 scenes analysis

Geological and tectonic interpretation and alteration zone extraction for each scene of the image were executed. Used for the analysis are LANDSAT TM false color synthetic image (BGR=145; scale 1: 250,000) and ratio images (BGR=3/1, 4/5, 5/7; scale 1:250,000). The description is made on geological unit classification, alteration zone distribution, lineament, folding structure and ring structure according to geological interpretation.

The result of geological and structural interpretation and alteration zone extraction was summarized into an interpretation map. On the geological stratigraphy, comparison was made with the geological maps of Chubut Province (scale = 1:750,000), Rio Negro Province (scale = 1:750,000), Neuquén Province (scale = 1:500,000), and Mendoza Province (scale = 1:500,000), and a Chilean geological map (scale = 1:1,000,000). The results are also shown in the tables. For details, refer to pp. 69-200 in the first fiscal year (phase 1) report (JICA/MMAJ, 2000).

b) Result of the analysis of mosaic image

(1) Geology unit

As a result of interpreting all the 13 scenes of the geologic image, the geology of this area was divided into 51 geologic units, comprising 35 units of the Paleozoic to Quaternary

sedimentary and volcanic rocks, 11 units of the Paleozoic to Tertiary intrusive rocks and 5 units of the Quaternary unsolidified sedimentary rocks. The details of geologic age and lithofacies are shown in Table II-2-2. Also, the comparative geologic stratigraphy among areas is summarized in Fig. II-2-2 and interpretation result over the entire area is summarized in Fig. II-2-3

As shown in Fig. II-2-2, a major characteristics of the geologic stratigraphy in the survey area is that the Triassic is not distributed in the southern half of the area, the Upper Cretaceous is not distributed in San Martin de Los Andes and Lago Menendez areas in the central west to the south of this area, and the Upper Tertiary system is not distributed only in the Lago Menendez area.

In the compilation of the 1:1,000,000 scale mosaic image, the rocks comprising the entire survey area were roughly divided into the following seven geologic units.

Table II-2-2 Geological age of 51 geological units of the mosaic image of the survey area.

Geological age	Geological unit	Geological age	Geological Unit	Intrusives	Geological unit
Quaternary	1 Qa	Cretaceous	1 Kss	Unknown	1 d
	2 Qt		2 Kss2	Unknown	2 dy
	3 Qsv		3 Kss1	Tertiary	3 αTm
	4 Qis3		4 Ksv		4 αTi
	5 Qis2		5 Kis2	Cretaceous	5 αK
	6 Qis1		6 Kis1	Tertiary-Cretaceous	6 αKT
	7 Qiva		7 Kiv	Tertiary-Cretaceous	7 αJT
	8 Qivb	Triassic	1 TRs	Jurassic	8 αJ
	9 Qivr		2 TRss		9 αJm
Tertiary	1 Tss		3 TRif	Triassic	10 αTR
	2 Tsv2		4 TRi	Paleozoic	11 αP
	3 Tsv1		5 TRiv	2nd suffix	
	4 Tsv	Carboniferous	1 Cv	I; inferior	
	5 Tms			m; middle	
	6 Tmv2			S;superior	
	7 Tmv1				
	8 Tmv	Proterozoic to Paleozoic	1 Ps	3rd suffix	
	9 Tiv			S; sedimentary rocks	
	10 Tis2			v; volcanic rocks	
	11 Tis1			F; pyroclastic rocks	
	12 Tis				

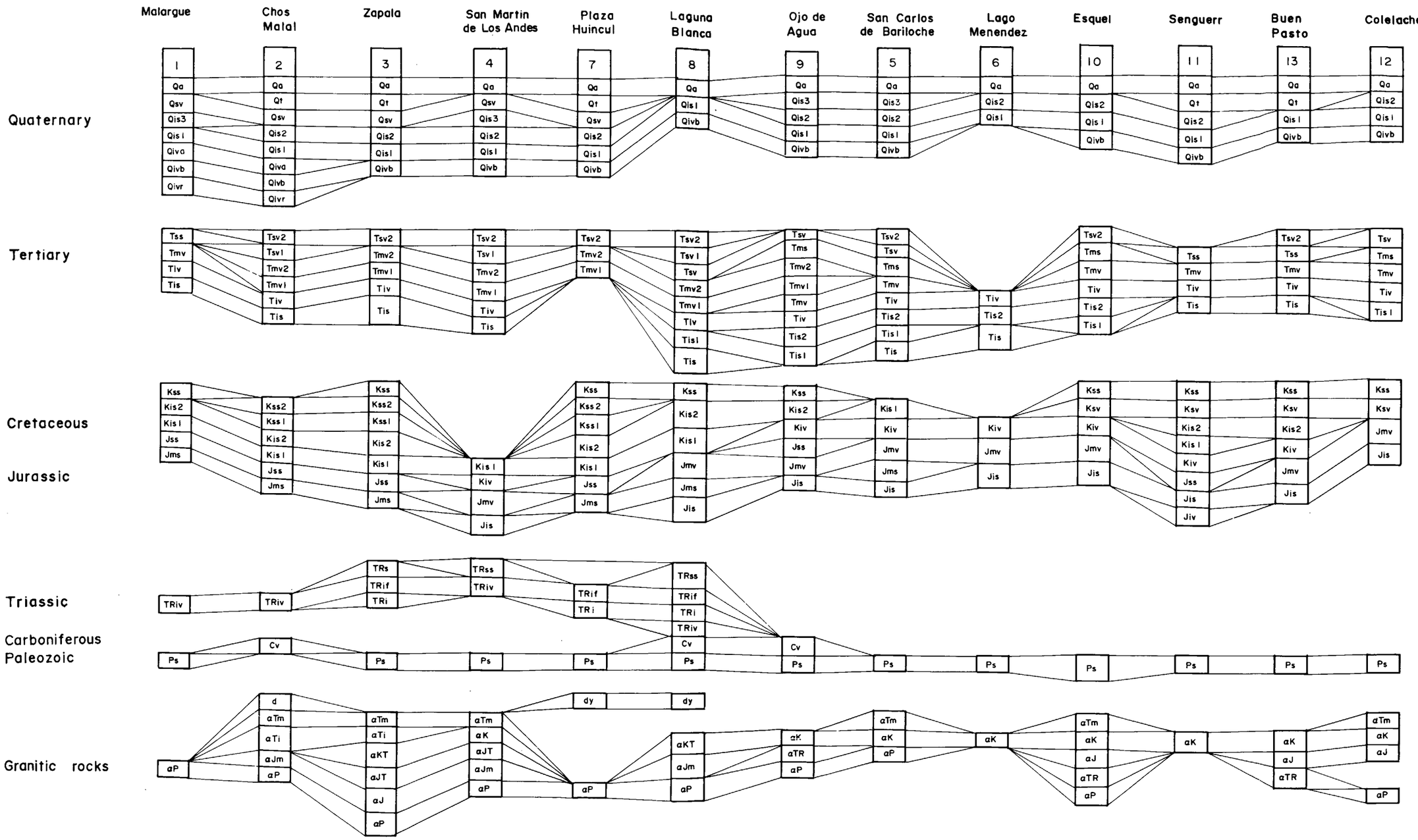

Fig. II-2-2 Stratigraphic correlation among the survey areas based on the interpretation maps

Legend

1. Q Quternany System
2. T Tertiary System
3. K Cretaceous System
4. J Jurassic System
5. TR Triassic System
6. C Carboniferous System
7. PS Undifferentiated Paleozoic Group
8. αTJK Jurassic to Tertiary Granitic Rocks
9. αP Paleozoic Granitic Rocks

- Alteration Zone
- Mineral Deposit
- Mineral showings
- Lineament Certain
- Lineament Uncertain
- Anticlinal Axis
- Synclinal Axis
- Annular Structure
- Lake

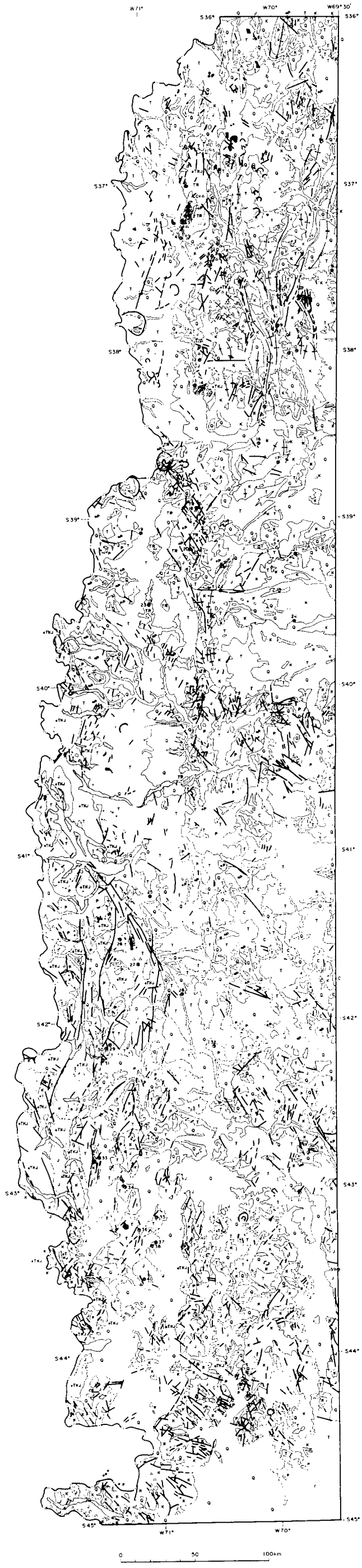

Fig. Ⅱ-2-3 Compiled photogeologic interpretation map of the survey area

① The Quaternary unsolidified sedimentary and volcanic rocks

They are primarily composed of unsolidified sediments, such as alluvium and diluvium (including glacial drifts) settling on topographically low lands, and volcanic rocks such as andesitic or basaltic rocks. They are extensively distributed in the northeast and south of the survey area. No alteration zones are observed.

② The Tertiary sedimentary and volcanic rocks

They are primarily volcanic rocks and develop with an extensive width of max. 35 km ± from the northwest to the southeast via the central east of the survey area. Sedimentary rocks, in addition to being distributed in a band trending toward NNW-SSE, are scattered around the center of the area. Numerous alteration zones were observed, especially in the volcanic rocks.

③ The Cretaceous sedimentary and volcanic rocks

They are divided into the northeast and southwest. The northeast is composed of sedimentary rocks and has repeated anticline and syncline tectonics generally trending toward N-S. In the southwest, volcanic rocks are dominant and intermittently continue generally in the NW-SE direction from the west of Epuyen city to Alto Rio Senguerr city via Esquel city. Numerous alteration zones were found in the volcanic rocks.

④ The Triassic sedimentary and volcanic rocks

They are scattered around the center of the north of this area in a band about 10 km wide from north to south. There are concentrated alteration zones in the west of Andacollo city and Zapala city.

⑤ The pre-Carboniferous sedimentary and volcanic rocks

They are primarily composed of the Proterozoic to Paleozoic schist which includes the Carboniferous pyroclastic rocks and sedimentary rocks. The Proterozoic to Paleozoic schist forms the basement of the survey area. They are distributed intermittently from the north end and San Martin de Los Andes city located at the center and from the west of Norquinco city in the south to Jose de San Martin city. Some small alteration zones were observed in the Paleozoic schist distributed in the west of Norquinco city.

⑥ The Triassic to Tertiary intrusive rocks

They exist mainly in the form of a band from north to south in the mountain area along the Chilean border. In addition, the Cretaceous intrusive rocks are scattered generally from Tecka city to Jose de San Martin city, and the Tertiary intrusive rocks are spread in the north and south of Chos Malal city. Many alteration zones were recognized.

⑦ The Paleozoic intrusive rocks

They are intermittently distributed generally trending toward NW-SE from the north of San Martin de Los Andes city to the east of Norquinco city. The occurrence is closely related to the pre-Carboniferous sedimentary rocks and volcanic rocks, and forms the basement of the survey area with the geologic unit of ⑤. Almost no alteration zones are observed.

(2) Alteration zones

The appearance of alteration zones extracted from the whole survey area are summarized in Table II-2-3. As the table shows, the total number of alteration zones is 244. By geologic unit, the largest number, 93 zones, is found in the Tertiary volcanic rocks, followed by 55 zones in the Jurassic to Tertiary intrusive rocks. Thirty zones were extracted from the Cretaceous volcanic rocks and 26 zones from the Jurassic

Table II-2-3 Number of alteration zones of 13 areas

Area	Total Number	Net Number ※	Number of alteration zones in each geological unit							
			Tv	Kv	Jv	TRv	Ps	αTKJ	αP	others
Malargue	20	20	18	0	0	0	0	0	1	1
Chos Malal	21	17	6	0	0	7	0	3	0	1
Zapala	37	37	14	0	0	18	0	0	5	0
San Martin de Los Andes	32	32	22	0	0	0	4	3	3	0
San Carlos de Bariloche	89	89	21	12	1	0	8	44	0	3
Lago Menendez	33	21	4	9	0	0	2	5	0	1
Plaza Huincul	9	1	0	0	0	1	0	0	0	0
Laguna Blanca	0	0	0	0	0	0	0	0	0	0
Ojo de Agua	25	9	3	0	0	0	3	0	1	2
Esquel	28	5	5	0	0	0	0	0	0	0
Senguerr	12	12	0	9	2	0	0	0	0	1
Colelache	5	0	0	0	0	0	0	0	0	0
Buen Pasto	7	1	0	0	1	0	0	0	0	0
Total	-	244	93	30	4	26	17	55	10	9

※ Net number after excepting alteration zones in overlapped area, Tv: Tertiary volcanics, Kv: Cretaceous volcanics, Jv: Jurassic volcanics, TRv: Triassic volcanics, Ps: Paleozoic sedimentary rocks, αKTJ: Jurassic to Tertiary intrusives, αP: Paleozoic intrusives volcanic rocks.

These alteration zones showed concentration generally trending toward N-S and can be grouped roughly into the following six concentrated areas:

① The north of Andacollo city: Seven concentrated areas
② Area in the west of Zapala
③ Area in the west of San Martin de Los Andes
④ Area of Norquinco to Esquel
⑤ Area in the southeast of Norquinco: Four concentrated areas
⑥ Area of Jose de San Martin to Alto Rio Senguerr: Four concentrated areas

(3) Fracture system

Numerous lineaments which suggest faults were extracted in the survey area. These lineaments were grouped into the following three regions based on direction and frequency of occurrence:

① Lat. 36° to 40° S

This region ranges from the northernmost limit of the survey area to its southernmost limit, i.e., 20 km to the north of San Martin de Andes city, and includes four highly concentrated zones of fracture. In these areas, lineaments trending toward N-S, NNE-SSW and NE-SW are prevailing. On the whole N-S lineaments are most predominant.

② Lat. 40° to 43° 30' S

This region covers from the southernmost limit of the above-mentioned area to the area near Tecka city and includes six highly concentrated zones of fracture. In these areas, lineaments trending toward N-S, NW-SE, NNE-SSW and E-W are prevailing. Three systems of lineaments, that is trending toward N-S, NW-SE and NNE-SSW, are influential on the whole.

③ Lat. 43° 30' to 45° S

This region covers from the southernmost limit of the above-mentioned area to the south end of this area, and includes zones of homogeneously high concentration of fractures except for areas around Tecka city and the east of Alto Rio Senguerr city. In this region lineaments trending toward WNW-ESE, NNW-SSE, N-S, ENE-WSW, E-W and NW-SE are recognized, and the lineaments are on the whole multi-directional.

A majority of alteration zones extracted in the analysis were located in highly concentrated zones of lineament within each region. This phenomenon suggests a close relationship between fractures and alteration zones both of which might have been developed with the formation of ore deposits.

2-2 Precise analysis of alteration zones

The aim of the satellite image analysis in this fiscal year (phase 2) is to classify alteration zones extracted from LANDSAT TM data. Many of the minerals composing alteration zones show absorption spectra that are characterisic of the short-wavelength infrared (IR) ranging 1.0 to 2.5 μm. This is caused by harmonics of normal vibrations of water molecules (H_2O), hydroxide ions (OH), carbonate ions (CO_3^{2-}) and sulfate ions (SO_4^{2-}) and also by the mixed vibration of them. Alteration minerals such as kaolinite and alunite can be presumed from distinctive features of this absorption spectra. Band 5 and band 7 of LANDSAT TM are optical sensors that have an observation wavelength in the short-wavelength IR.

Rock and soil distributed on the ground surface comprise a mixture of various kinds of minerals. If kinds and quantitative ratios of minerals composing rock and soil can be determined, it is possible to identify alteration and non-alteration zone and also to know what kind of alteration minerals occur in the alteration zone.

The iso-grain model (Hiroi and Pieters, 1992) is a theoretical model to accurately estimate the quantitative ratio (volume ratio) of minerals composing the mixture based on the reflectance of the powdery mixture if the composition of minerals are known. In this analysis, we decided to determine the kind and quantitative ratio of minerals distributed on the ground surface by using the iso-grain model.

2-2-1 Data used

The subject of the analysis is LANDSAT TM images of six scenes including promising zones extracted in the first fiscal year (phase 1) survey being selected from 13 scenes of the whole survey area (Fig. II-2-1). Table II-2-4 shows relevant information, such as dates when images of the six scenes were observed and the position of the sun.

Table II-2-4 Path/Row, date of acquisition, sun azimuth and sun elevation of 6 scenes of LANDSAT TM image of for detailed analysis

No.	Name of the scene (area)	Path	Row	Date of acquisition	Sun azimuth	Sun elevation
1	Malargue	232	85	Feb. 9, 1987	75°	44°
2	Chos Malal	232	86	Feb. 9, 1987	74°	44°
3	Zapala	232	87	Feb. 9, 1987	73°	43°
5	San Carlos de Bariloche	232	89	Feb. 22, 1986	65°	40°
6	Lago Menendez	232	90	Dec. 7, 1986	73°	50°
10	Esquel	231	90	Jan. 27, 1985	71°	46°

2-2-2 Methods of image processing and preparation

The methods of image processing and preparation conducted in this fiscal year are described in as follows:

1) Radiance and pseudo reflectance

In order to judge what minerals are distributed on the ground surface from the satellite data by the use of the iso-grain model, it is necessary to convert the DN (digital number: integral number from 0 to 255 in the case of the LANDSAT TM) of the satellite data to pseudo reflectance. Only the pseudo reflectance rather than reflectance can be found from DN for the following reason.

It is assumed that the ground surface consists of one kind of powdery mineral. It is also assumed that each grain of powdery mineral is sufficiently minute and the surface of the grains faces to all directions. Considering reflection of two direction at a certain wavelength (the direction and angle of incidence of light to a sample and the position of a measuring instrument are fixed), values of radiance incident upon the instrument measuring brightness change when positions of the light source and the instrument change.

The area of the ground surface that the satellite is looking at as a pixel is constant, and the volume (wavelength) of light energy entering this scope of a pixel depends on the angle between the ground surface and the sun (on the assumption that transmittance of the air is constant regardless location). Where the energy of incidence to the unit plane that is perpendicular to the direction of incidence of the sun is "S", and the angle between the ground surface and the direction of incidence is "Q," the energy of incidence to the unit ground surface can be then expressed as "S*cosQ."

It is assumed that grains of powdery mineral face to all directions. When light reaches the ground surface, complete to incomplete mirror reflections occur on the surface of each mineral. Moreover, mirror reflection of both reflecting and transmitting lights occurs. All reflection constituents from the ground surface are made up of mirror reflection in this

manner. The energy reflectance of mirror reflection is determined by the angle between the mineral surface and incidence light as well as by the refractive index of minerals (Frenel's equation). Therefore, it is known that reflection energy from powdery body at a certain wavelength (with a fixed refractive index) changes according to the angles of incidence. With a fixed angle of incidence, three-dimensional distribution of reflection energy is the strongest at the position of mirror reflection.

Angles between incident light from the sun and the ground surface, and between the ground surface and the direction of satellite observation vary with a position on the ground surface. This shows that radiance to the direction of the satellite from each point is not constant because the angle between the ground surface and the sun or the satellite is different even if the ground surface consists of the same material. The influence exerted by these angles upon radiance is considered to be uniform even if the wavelengths are different. Therefore, if an angle between the ground surface and the sun or the satellite is known, it is possible to convert radiance to reflectance.

However, it is difficult to know the direction of inclination of the ground surface at each position. Since the influence exerted by the angle between the ground surface and the sun or the satellite upon radiance does not depend on wavelength, it is possible to determine pseudo reflectance from radiance at each wavelength based on the assumption that reflectance at each wavelength multiplied by a certain value is the pseudo reflectance.

2) Determination of the path radiance value

In the LANDSAT TM, the observed radiance (unit of which is mW/cm^2sr) is output as a DN. Because the DN corrected on the ground has a linear relationship with observed radiance at the satellite, absolute radiance of the LANDSAT TM can be found from the following equation.

$$R = (R_{max} - R_{min}) * V/D_{max} + R_{min} \qquad ①$$

Here, "D_{max}" is 255 (the largest DN), "V" is a corrected DN, "R" is the absolute radiance at that time, and "R_{max}" and "R_{min}" are the largest and smallest radiance values of the detector, respectively (Remote Sensing Technical Center, 1990). Upward radiation from the ground surface that reaches the satellite is expressed by the following formula.

$$I_n = (I_S)_n T_n + P_n \qquad ②$$

An accompanying component of Formula ②, "n," is a band number of the sensor, and "I_n" and "$(I_S)_n$" are the radiance reaching the satellite and radiance on the ground surface,

respectively. "T_n" is the transmittance of the air, and "P_n" is a scattered light from the atmosphere that reaches the satellite, which is called path radiance and must be removed in order to obtain information on conditions of the ground surface (Tsuchiya, ed., 1993).

Estimates of path radiance in each band were made as follows: It was assumed that there were points where the radiance on the surface is 0 or can be deemed to be 0 in the target area. In this case, radiance that has reached the satellite is path radiance only. Since it is assumed that path radiance is uniform in the whole target area, radiance reaching the satellite is the smallest value of the whole in this case; namely, the smallest DN.

There are more than 50,000,000 pixels in each scene, and an cumulative curve of the distribution of DN values can be obtained (Fig. II-2-4). In order to find the smallest value of about 50,000,000 pixels, points where a curve changes to a straight line in the section with small DN values were selected, the line was extended to smaller DN values, and then a value representing accumulated probability density near the section "{accumulative frequency}=1" was regarded as the smallest one (Fig. II-2-4).

Path radiance (the smallest value of brightness) was estimated by obtaining cumulative curve of the distribution classified by the band of each scene. The values of path radiance in each band are shown in Table II-2-5.

Table II-2-5 Path Radiance (minimum DN)

Path:Row	DN1min	DN2min	DN3min	DN4min	DN5min	DN7min
P232:R85	43	12	7	2	-1	-4
P232:R86	43	12	7	2	-1	-4
P232:R87	43	12	7	2	-1	-4
P232:R89	40	10	5	1	-2	-4
P232:R90	52	12	8	1	-3	-5
P231:R90	48	13	9	3	-1	-4

3) Preparation of scatter diagrams

Dispersion diagrams of two constituents of DNs in each band, where values of path radiance were deducted as explained in the preceding section, were prepared (Fig. II-2-5). Reflectance of almost all soil and rock is between red of visible (band 3) and near IR (band 4), and shows a pattern of gentle spectral reflectance. With a dispersion diagram between these two bands prepared, plants are plotted on the side close to the near IR because reflection of band 4 is strong. On the other hand, soil and rock concentrate in the periphery of a regression line with a fixed inclination because a correlation between the two bands is very high. Such a linear distribution pattern shown by soil and rock is called the soil line (Saito et al. 1998).

4) Removal of areas with cloud, snow and water

In order to confirm the areas with cloud, snow and water false color image (BGR= 754) was produced for six scenes shown in Table II-2-4. In false color image with this color combination, the area covered with cloud is expressed in white to cream, the snow cover is red and the water is dark black. Conditions used for removal of areas with cloud, snow and water are described below.

Area with cloud : DN1>200 ∩ DN5>100 ∩ DN7<96 ③

Area with snow : (DN1>200 ∩ DN5≦100)
∩
(DN7<96 ∩ (DN5-DN5min)/(DN2-DN2min) < dip 25) ④

Area with water : (DN5+DN7<20 ∪ DN5<7)
∪
(DN7<7 ∪ (DN5-DN5min)/(DN2-DN2min) < dip 25) ⑤

As a result of examination on dispersion diagrams between bands and false color images, areas with the snow cover and the bared rock were separated to the greatest extent in a dispersion diagram of band 2 and band 5. "Dip 25" is a threshold of the ratio between values that are obtained by subtracting the smallest value of band 2 and band 5 from both values. Table II-2-6 shows "dip 25" used for each scene. As data of three scenes from P232/R85 to R87 were successively obtained, their thresholds are equal.

Table II-2-6 Value of dip 25

Path:Row	P232:R85	P232:R86	P232:R87	P232:R89	P232:R90	P231:R90
dip 25	1.230	1.230	1.230	1.620	1.931	1.390

5) Removal and processing of the vegetation area

A soil line mentioned above is determined from a dispersion diagram of band 3 and band 4 of the image after removing effects of cloud, snow and water, and the inclination is calculated (Fig. II-2-7). This inclination is called "dip 34" and a straight line on the dispersion diagram expressed by the following formula are regarded as the percentage of vegetational cover to be 0% (See Fig. II-2-7).

DN4 = dip 34*DN3 ⑥

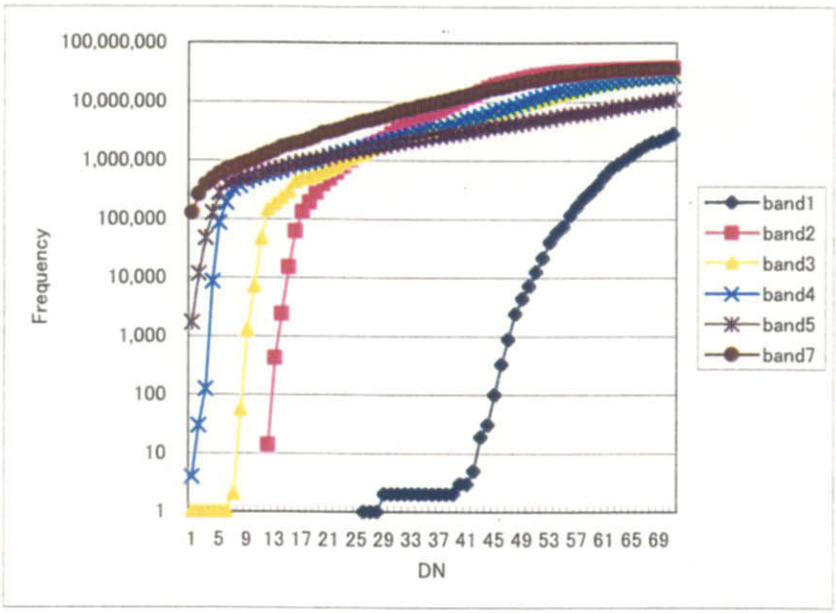

Fig. II-2-4 Cumulative curve of DN of LANDSAT TM data (P232/R085)

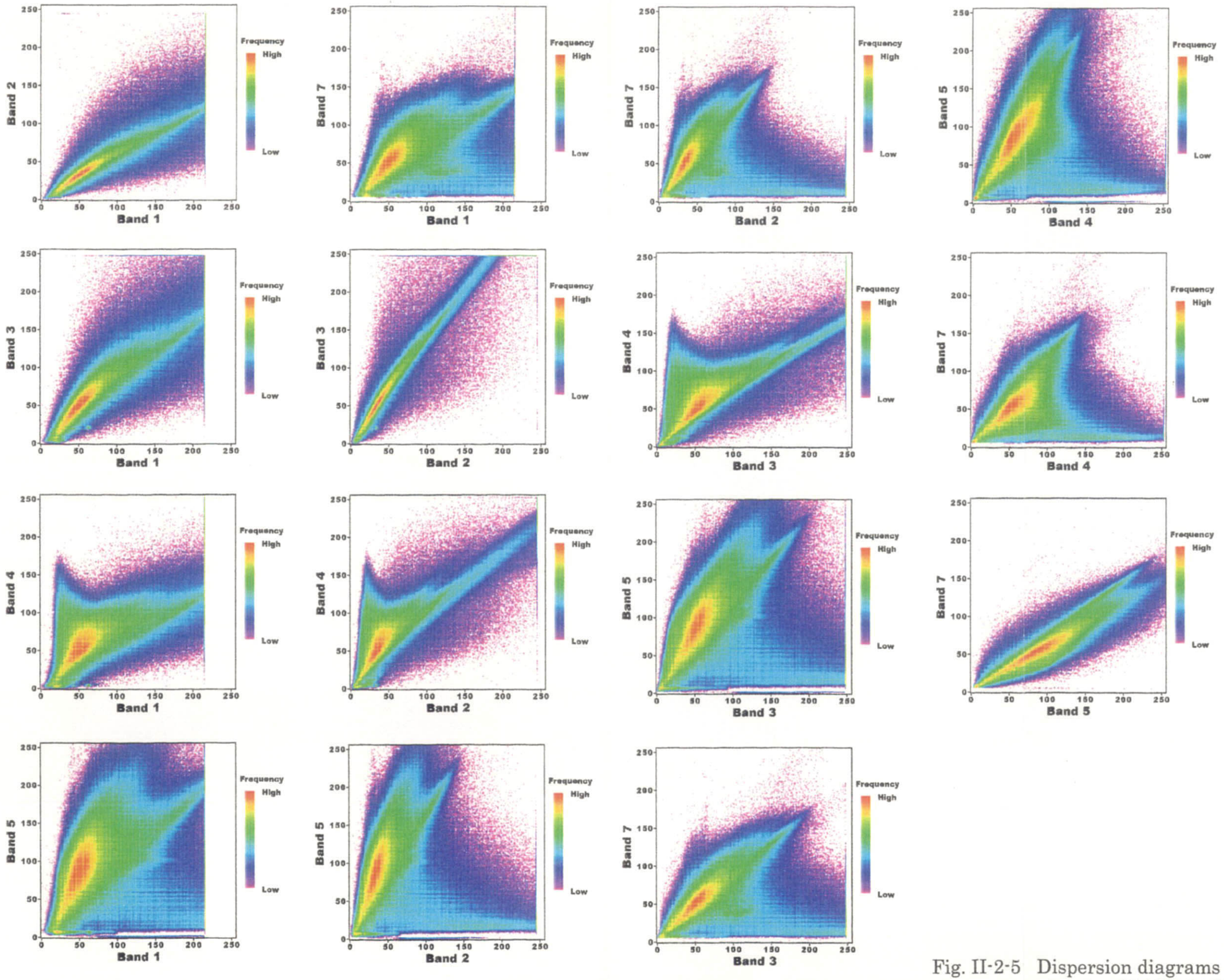

Fig. II-2-5 Dispersion diagrams of DN between two bands of LANDSAT TM data

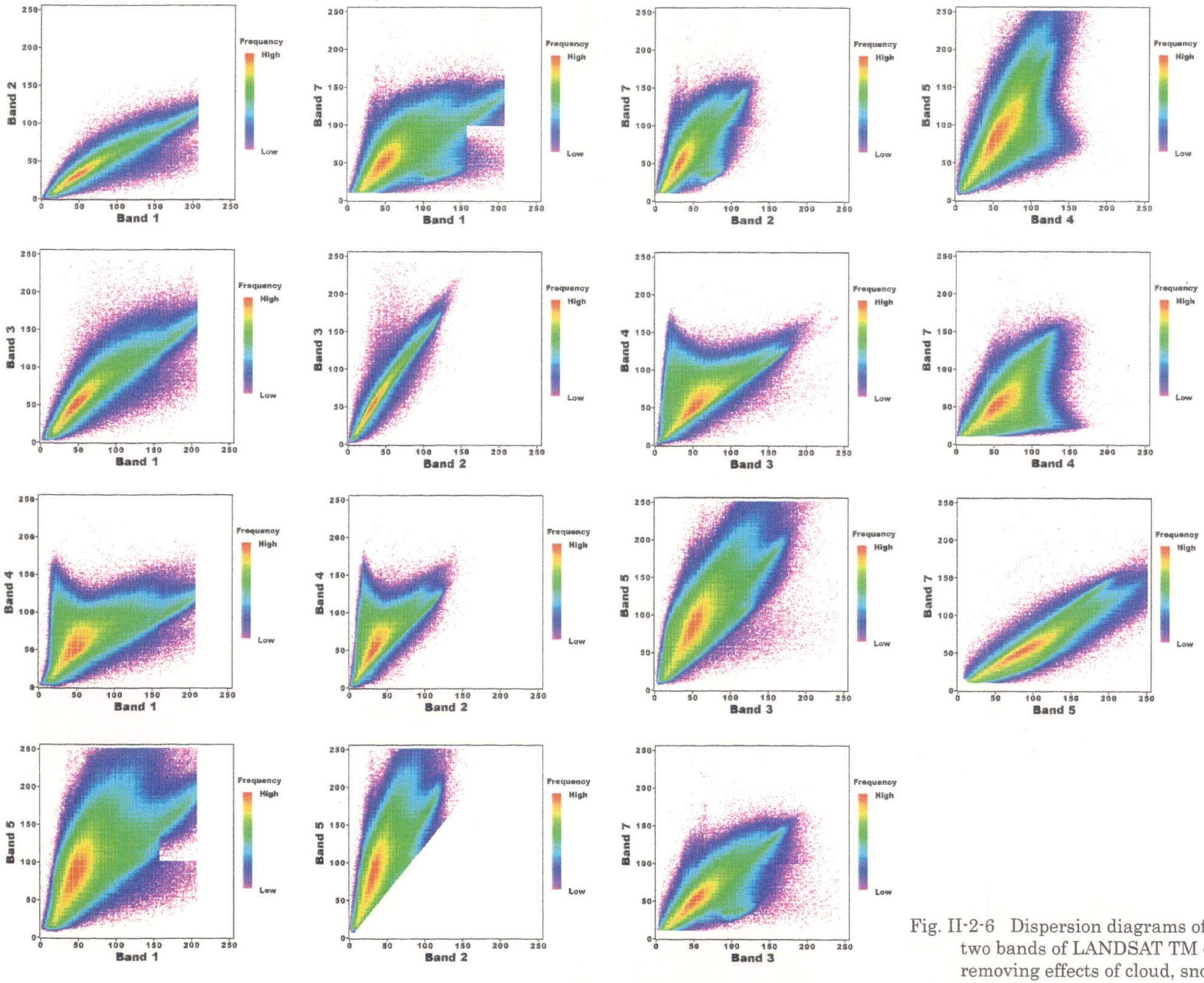

Fig. II-2-6 Dispersion diagrams of DN between two bands of LANDSAT TM data after removing effects of cloud, snow and water

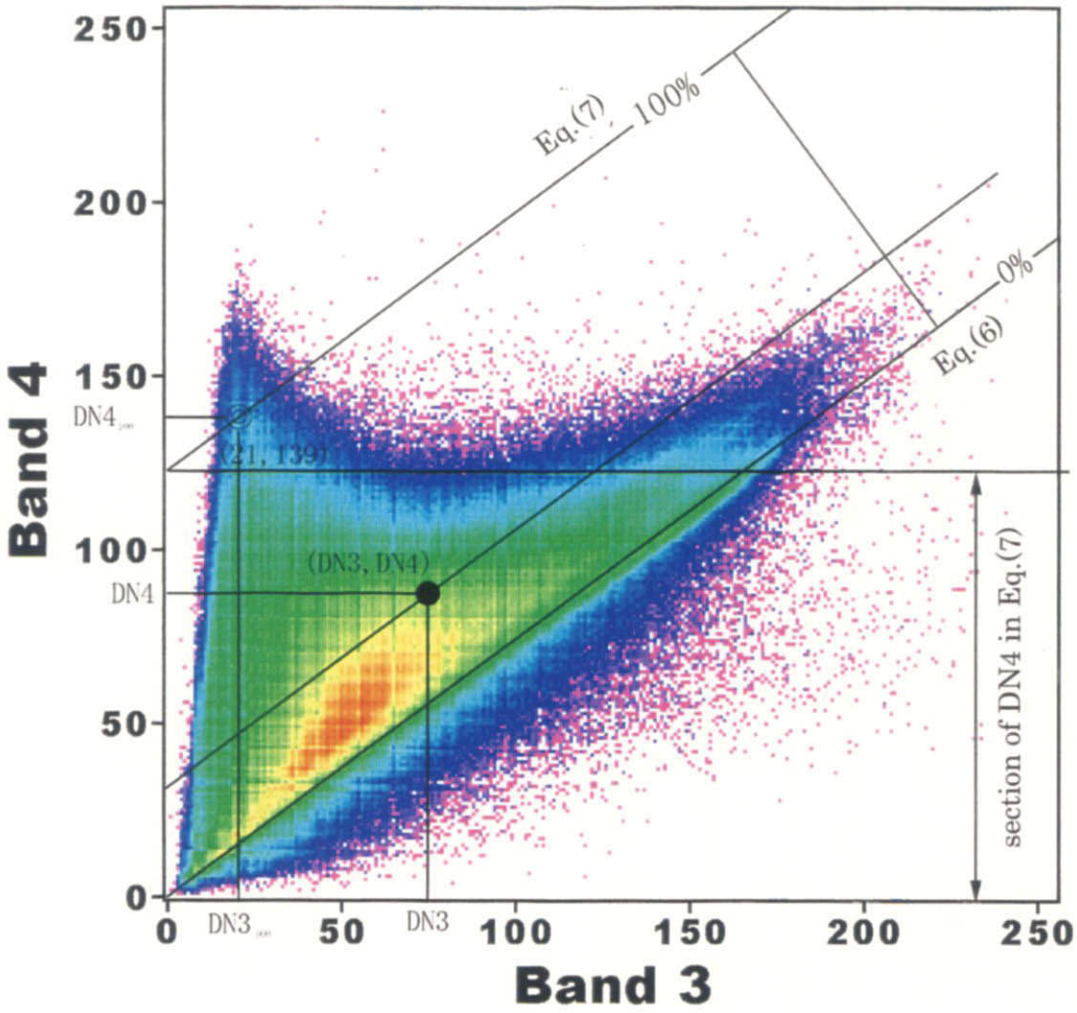

Fig. II-2-7 Dispersion diagram of DN between Band 3 and Band 4 of LANDSAT TM data for removing effects of vegetation

Next, the percentage of vegetational cover around the apex of a triangle, the base of which is the soil line, is regarded as 100%; the average DN value of each band around this point is designated "DNi_{100} (i = 1,2,3,4,5,7) ". The equation of the straight line that passes through the point of 100% vegetational cover and is parallel to the soil line is as follows:

$$DN4 = dip\ 34*(DN3 - DN3_{100}) + DN4_{100} \qquad ⑦$$

The DN4 intercept of the equation shown above and the DN4 intercept (origin) of the soil line are made to correspond to vegetational cover of 100% and 0%, respectively. The rate of vegetational cover of any pixel, V, can thus be expressed by the equation shown below.

$$V = (DN4 - DN3*dip\ 34)/(DN4_{100} - dip\ 34*DN3_{100})*100 \qquad ⑧$$

The DN of each band is converted to DN so that the rate of vegetational cover is supposedly 0%. This conversion is executed according to the following equation.

$$DNi_0 = (DNi - V/100*DNi_{100})/(1 - V/100) \qquad ⑨$$
$$i = 1, 2, 3, 4, 5, 7$$

Table II-2-7 shows the thresholds of the percentage of vegetational cover used for each scene, dip 34 and DNi_{100}.

Table II-2-7 Threshold, dip 34 and DNi_{100} of vegetated area in 6 scenes

Path:Row	Threshold(%)	dip34	$DN1_{100}$	$DN2_{100}$	$DN3_{100}$	$DN4_{100}$	$DN5_{100}$	$DN7_{100}$
P232:R85	20	0.788	26	21	21	139	80	30
P232:R86	20	0.788	26	21	21	139	80	30
P232:R87	10	0.788	26	21	21	139	80	30
P232:R89	4	0.810	26	18	17	149	85	26
P232:R90	5	0.861	30	23	20	167	94	30
P231:R90	5	0.843	23	16	15	148	81	26

6) Extraction of alteration zones

In order to highlight pixels of alteration zones, we first referred to images with bands 1, 5 and 7. However, problems occurred with this method, for example, salt-lake-deposits were regarded as an alteration zone, and weak alteration zones could not be detected. To overcome these problems and secure consistency with the interpretation result of the first fiscal year (phase 1) survey, we tried to extract pixels of alteration zones by imposing some conditions on the ratio image used for the phase 1 survey. As a result, it was concluded that extraction

should be carried out by changing threshold of extracting alteration zones according to the scene of image.

Color combination of the ratio image used for the interpretation in the first fiscal year is band 3/band 1 (B), band 4/band 5 (G) and band 5/band 7 (R). The ratio value of each combination, that is R_{31}, R_{45} and R_{57}, can be expressed as follows:

$$R_{31} = (DN3 - DN3min)/(DN1 - DN1min)$$
$$R_{45} = (DN4 - DN4min)/(DN5 - DN5min)$$
$$R_{57} = (DN5 - DN5min)/(DN7 - DN7min) \quad ⑩$$

Because any of values from 0 to 10 is usually taken as a ratio value, it is converted to a value between 0 and 255 on a gain bias when producing the ratio image. Fig II-2-8 shows the frequency distribution of ratio values of the scene of P232/R087.

This conversion was made with the following equation based on frequency distribution.

$$Y_{31} = R_{31}*300 - 405$$
$$Y_{45} = R_{45}*425 - 170$$
$$Y_{57} = R_{57}*400 - 340 \quad ⑪$$

Formula ⑪ is a linear conversion to make the highest and lowest values of distributions of R_{31}, R_{45} and R_{57} (positive real number) correspond to 255 and 0 respectively. Here, values 300, 425 and 400 show sensitivity, and -405, -170 and -340 are the bias. For Y_{31}, Y_{45} and Y_{57} obtained from Formula ⑪, pixels that satisfy the conditions of Formula ⑫ were regarded as alteration zones. Y_{1min}, Y_{2max} and Y_{3min} are thresholds. The threshold value used for each scene is shown in Table II-2-7.

$$Y_{31}>Y_{1min} \cap Y_{45}<Y_{2max} \cap Y_{57}>Y_{3min} \quad ⑫$$

Table II-2-8 Threshold for extracting alteration zones

Path:Row	P232:R85	P232:R86	P232:R87	P232:R89	P232:R90	P231:R90
Y_{1min}	150	150	130	110	110	110
Y_{2max}	90	90	300	130	130	130
Y_{3min}	150	150	130	110	110	110

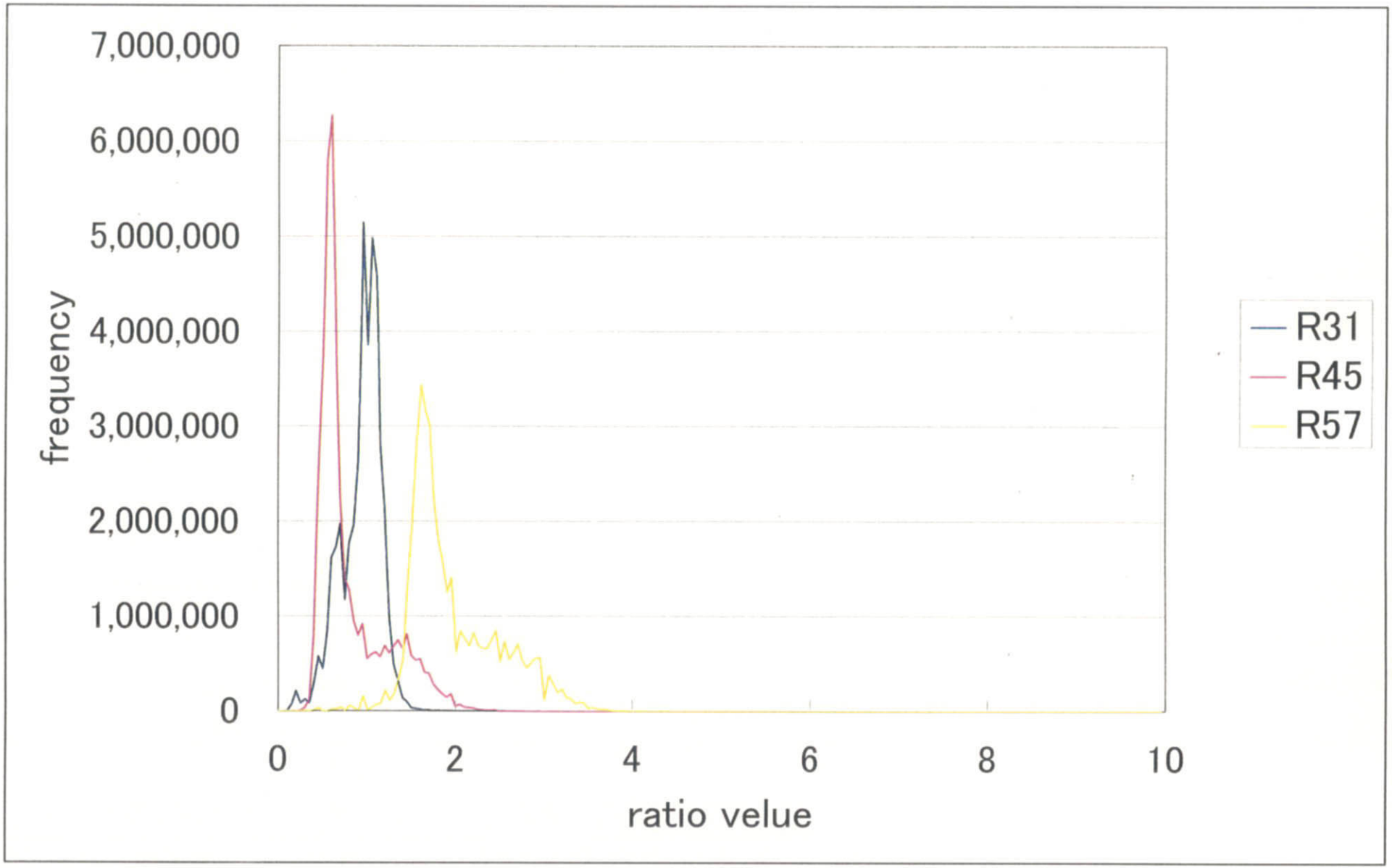

Fig. II-2-8 Frequency distribution of ratio value of LANDSAT TM data (P232/R087)

7) Method of conversion to pseudo reflectance

The well-known methods of conversion to pseudo reflectance are as follows:

(i) Method in which reflectance is compared with brightness when reflectance of a pixel is known
(ii) Method in which the largest brightness of each band over the entire scene is adjusted to reflectance of 100%
(iii) Method in which the average brightness of each band over the entire scene is adjusted to reflectance of 100%

Method (i) is the most accurate. The existence of pixel whose reflectance is known, however, is generally rare, and this method cannot be used in this survey area. Methods (ii) and (iii) can be used only when judging whether or not specific minerals with strong absorption spectra exist in case that such minerals are extremely concentrated and distributed on the ground surface. However, it is theoretically impossible to obtain a level of accuracy that can be fit for judgement of the quantitative ratio of constituents of general altered rocks. Therefore the following method is adopted here.

a) Soil line of soil and rock samples

The average reflectance was calculated at the wavelength that was fit to wavelength range of the LANDSAT TM, after collecting data (about 200 samples) on reflectance of soil and weathered rock which was actually measured by indoor spectral analysis. Dispersion diagrams of reflectance between two bands were then prepared from this data (Fig. II-2-10).

In the images used for this analysis, vegetation is more dominant towards the south. In order to obtain data with as high correlation between bands as the indoor spectral analysis, it is necessary to strictly remove pixels which are affected by vegetation.

b) Conversion coefficient

At the beginning, the results of conversion of reflectance of pixels with low brightness (such as the shady part of a mountain) were unstable, and the resultant judgement of minerals also lacked appropriateness. Therefore, after removal of pixels of areas with cloud, snow, water and vegetation, data excluding the following pixels was examined.

* alteration zones
* pixels under a certain threshold of each band
* pixels of "DNi>250" in each band (removal of data which may be saturated with the received energy)

Pixels that are not included in the above-mentioned removal have not been over-sampled and have high brightness in every band. Among 200 soil and mineral reference samples, only quartz is considered to have such a characteristics. Therefore, reflectance data of quartz, instead of mixture with other material, was employed as a reference sample to determine a conversion coefficient.

In the actual process, on a dispersion diagram after removing effects of cloud, snow and water, a soil line passing through the center of distribution was assumed in the direction of the tail of distribution most distant from the origin (Fig. II-2-10). Then brightness ratio between bands in the image was calculated. A conversion coefficient is determined so that the product of brightness ratio (inclination of the soil line) by the conversion coefficient is equal to the reflectance ratio of quartz between bands. Table II-2-9 shows the conversion coefficient used for each scene.

Table II-2-9 Transform coefficient used in 6 scenes

Path:Row	Band 1	Band 2	Band 3	Band 4	Band 5	Band 7
P232:R085	0.325	0.544	0.357	0.430	0.305	0.640
P232:R086	0.325	0.544	0.357	0.430	0.305	0.640
P232:R087	0.325	0.544	0.357	0.430	0.305	0.640
P232:R089	0.359	0.544	0.358	0.432	0.257	0.530
P232:R090	0.318	0.538	0.383	0.450	0.259	0.580
P231:R090	0.348	0.553	0.358	0.422	0.269	0.593

8) Classification of alteration zones

Semi-quantitative identification of alteration minerals was tried which combines synthesis of pseudo reflectance spectrum using iso-grain model (Hiroi et al., 1985, Hiroi and Takeda, 1989; Hiroi and Pieters, 1992) and pattern matching

a) Preparation of the reflectance spectrum index of alteration minerals

In the iso-grain model, if the surface reflectance and absorption ratio in each wavelength zone of a certain mineral group are given, the calculated reflectance in each wavelength is expressed as a function of the volume ratio and particle size of minerals, as shown below.

$$X_\lambda = f_\lambda(q_1, q_2, q_3, \cdots\cdots, q_n, d_1, d_2, d_3, \cdots\cdots, d_n) \quad ⑬$$

X_λ: calculated reflectance at wavelength λ

q_i: volume ratio of each mineral

d_i: grain size of each mineral

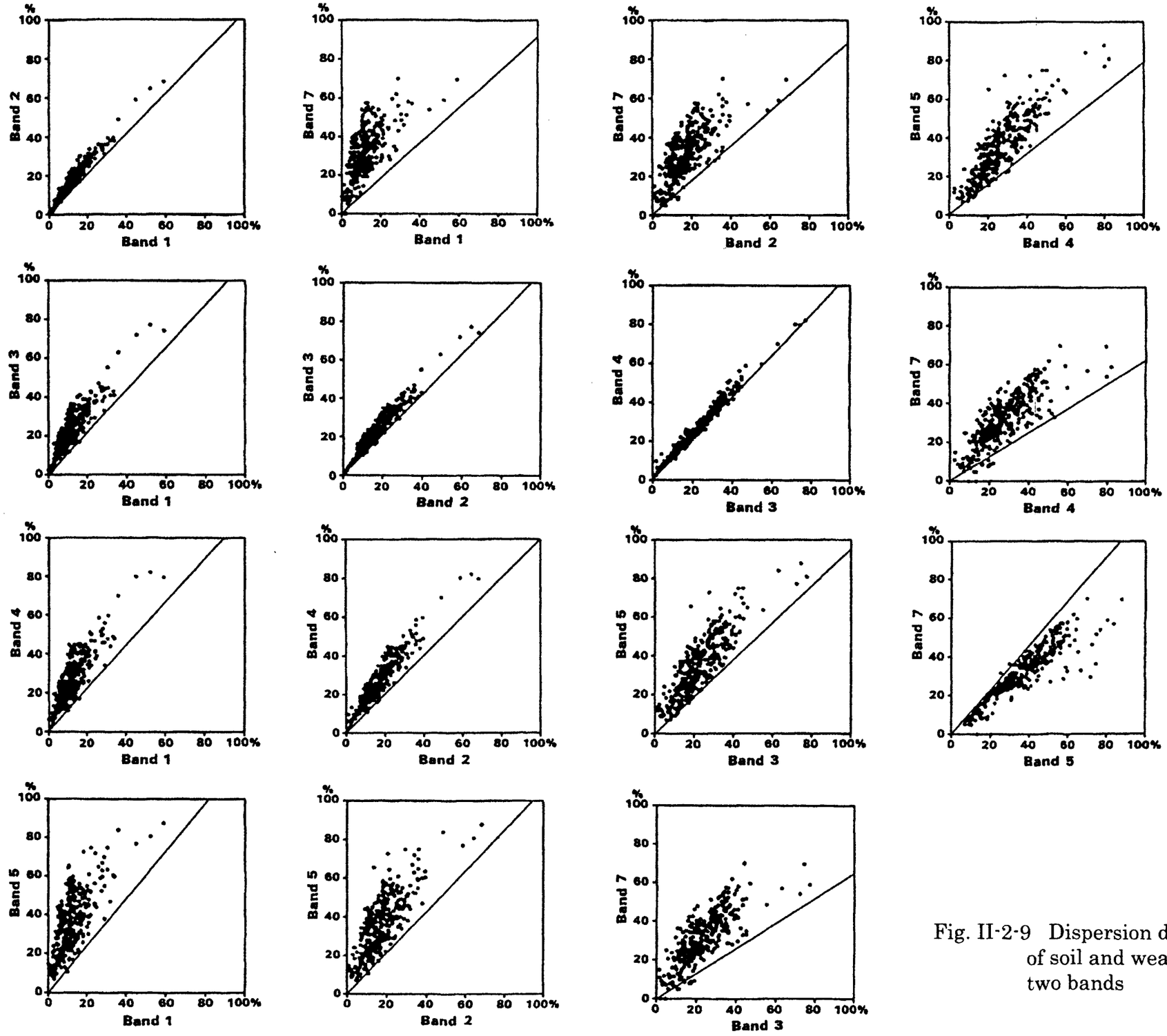

Fig. II-2-9 Dispersion diagrams of reflectance of soil and weathered rock between two bands

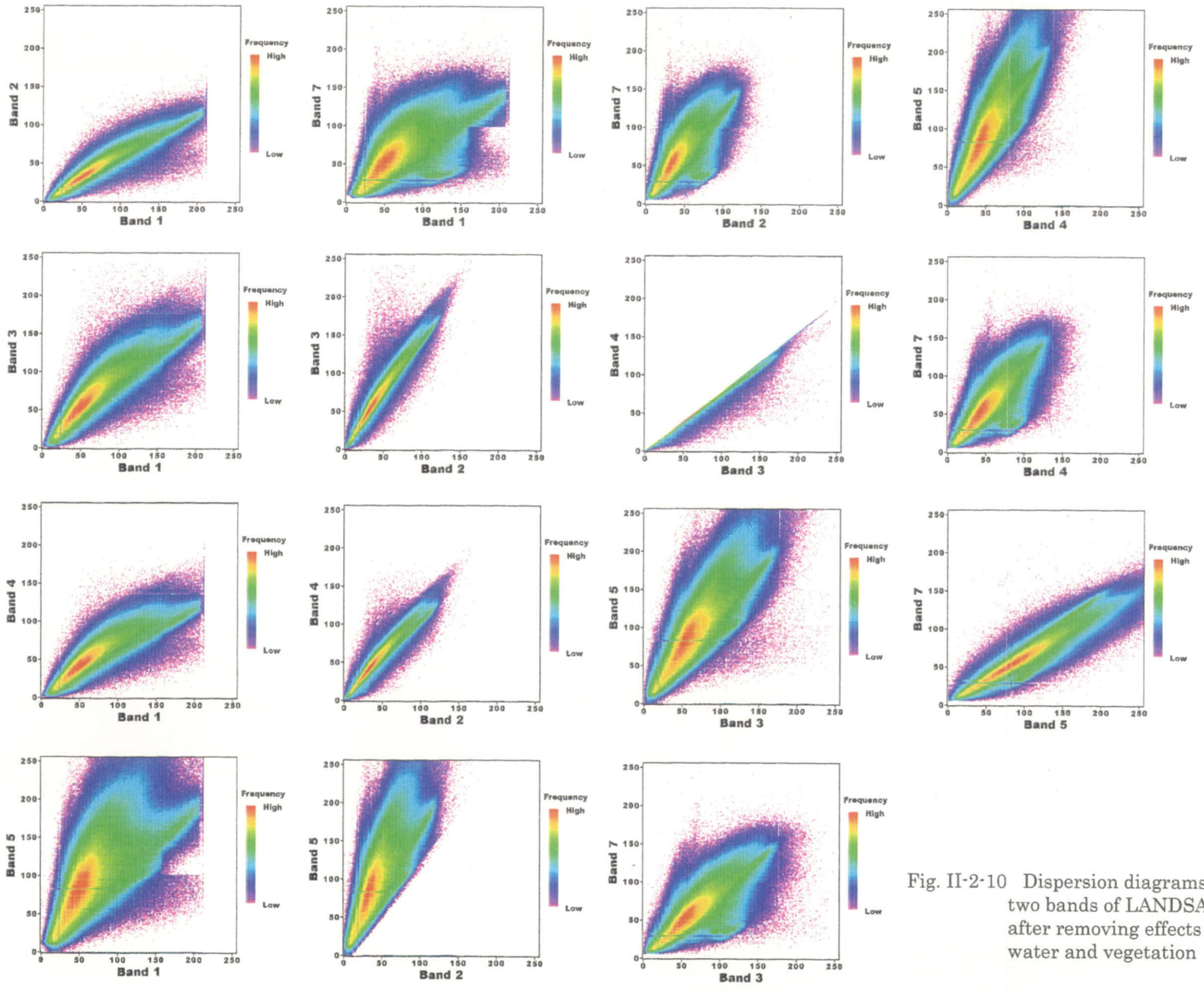

Fig. II-2-10 Dispersion diagrams of DN between two bands of LANDSAT TM data after removing effects of cloud, snow, water and vegetation

Therefore, on the assumption of particle size, if the number of observed wavelengths is "n", the volume ratio of "n" minerals can be found by solving an equation of the wavelength of "n". Because it takes much time to perform this calculation for individual pixel, however, this can not be an effective method. For this reason, we made, in advance, an index by calculating pseudo reflectance where minerals were mixed with various volume ratios. We then carried out classification of alteration minerals by comparing the index with pseudo reflectance of each pixel which has already been extracted by the threshold of alteration zone.

The distinctive features of this method are that reference takes a relatively short time and the kind of minerals can be set without limitation of the number of wavelengths because it is not necessary to solve the equation. It is, however, necessary to consider that reliability of the result of reference will lower if a large number of minerals are given as a variable for the number of wavelengths.

In this analysis, the following two kinds of indexes were compared. Index 1 contains neutral to alkali alteration minerals, and Index 2 contains acid alteration minerals. Fig. II-2-11 shows spectral pattern of six minerals of Index 1 and Index 2.

As a result of mixing proportion of each mineral being set at every 10%, calculated reflectance spectral pattern increases up to 3,003 both in Index 1 and Index 2.

b) Change of reflectance spectra when two phases of minerals are mixed

When two-phase alteration minerals are mixed, a reflectance spectrum changes non-linearly to the volume ratio. Fig. II-2-12 shows changes of the reflectance spectrum when two kinds of alteration minerals are selected from nine minerals and the mixed proportion is changed at every 20%. In this figure, mineral assemblages where spectra change linearly to the mixed proportion are goethite-montmorillonite, goethite-sericite, alunite-gypsum, and goethite-kaolin. On the other hand in the assemblages of goethite-gypsum and goethite-alunite an influence of goethite is large, while an influence of kaolin is large in case of kaolin-alunite assemblage. As a result of mixture of a small proportion of goethite in the former assemblage and of kaolin in the latter, the reflectance spectrum becomes close to that with the mixed proportion of 100%.

c) Judgement

A comparison of indexes obtained as mentioned above with pseudo reflectance obtained from the images are made by pattern matching. The conversion coefficient calculated in the preceding section is to correct the brightness ratio between bands and not a conversion coefficient to the absolute reflectance. In other words, the converted brightness ratio shows only a relative relationship based on the brightness value of band 1. The observed brightness value differs even if the substance on the ground is the same since the volume of incident

light to the ground surface is different due to topographical relief. Therefore, it is impossible to directly compare the product of brightness of an image by the coefficient with an index. For this reason, the conversion to pseudo reflectance was carried out by converting the intensity of pseudo reflectance to a direction cosine.

Pseudo reflectance, R_i (i = 1, 2, 3, 4, 5, 7), is expressed by the equation shown below.

$$R_i = I_i / (\Sigma I_j^2)^{1/2} \qquad ⑭$$

"I_j (j = 1, 2, 3, 4, 5, 7)" is a numerical value obtained by multiplying the brightness value of each pixel by the conversion coefficient.

On the other hand, a calculated pseudo reflectance with alteration minerals being mixed in the preceding section is also converted to a direction cosine. These steps allow the calculated pseudo reflectance of alteration minerals to be directly compared with the pseudo reflectance of each pixel of the image. When sum of squares of the difference between the two pseudo reflectance becomes minimum, we determine the calculated pseudo reflectance to be the most fitted spectra. An example of the results of the judgement is shown in Fig. II-2-13.

9) Geometrical conversion

Geometrical conversion was executed for each scene after extracting alteration zones and judging type of alteration minerals. Fourteen to twenty GCPs (ground control points) were selected from the GIS data used in each scene, and geometrical conversion to the UTM coordinate was carried out. The GCPs were selected at the meeting or bending points of rivers and the projection or pointed ends of bank of lakes.

LANDSAT TM images displaying results of classification of alteration minerals after executing geometrical conversion are shown in Figs. II-2-14a to f. In these images degree of the fit is expressed in green for Index 1 and yellow for Index 2. Outline of alteration zone visually extracted from the ratio image in the first fiscal year (phase 1) survey were shown in red.

2-2-3 Results of diagnosis and analysis of images

Results of diagnosis and analysis of images in six scenes are summarized below. Here, the alteration zones visually extracted from the ratio image in the first fiscal year (phase 1) survey are called "alteration zones[1]" and those extracted from alteration zone precise analysis of this year (Index 1, Index 2) are called "alteration zones[2]."

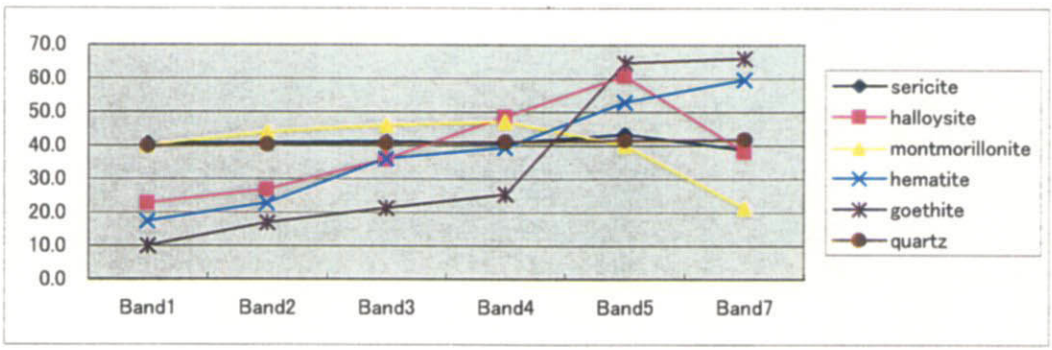

Index 1 : quartz, goethite, hematite, montmorillonite, halloysite, sericite

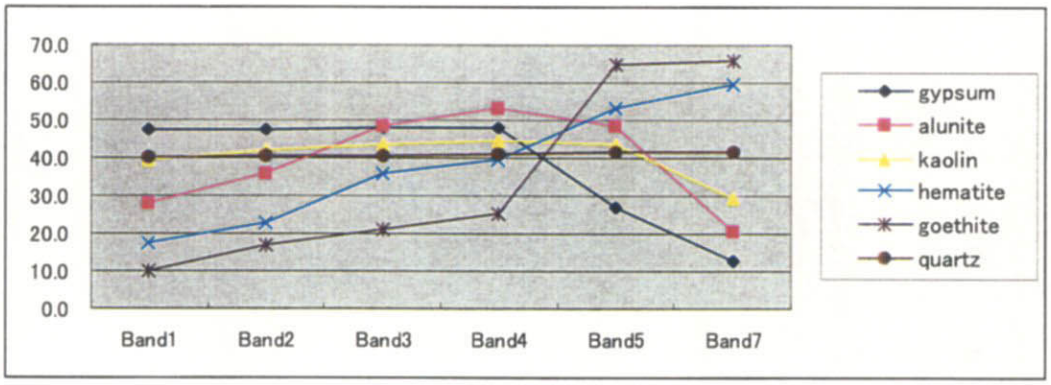

Index 2 : quartz, goethite, hematite, kaolin, alunite, gypsum

Fig. II-2-11 Spectral pattern of six minerals of Index 1 and Index 2

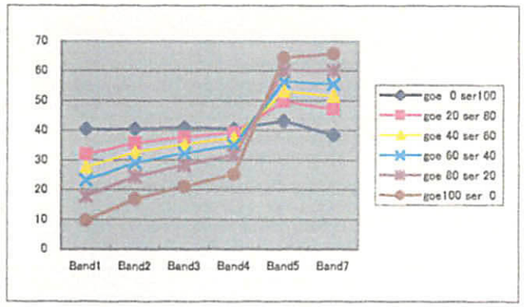

Mixed phase of goethite and sericite									Band1	Band2	Band3	Band4	Band5	Band7
0	0	0	0	0	100	goe 0	ser100		40.5	40.7	41.1	40.6	43.3	38.6
0	20	0	0	0	80	goe 20	ser 80		32.0	35.8	37.9	39.3	49.8	47.2
0	40	0	0	0	60	goe 40	ser 60		27.7	32.7	35.4	37.6	53.3	51.6
0	60	0	0	0	40	goe 60	ser 40		23.3	29.2	32.5	35.3	56.6	55.7
0	80	0	0	0	20	goe 80	ser 20		17.9	24.6	28.4	31.8	60.2	60.3
0	100	0	0	0	0	goe100	ser 0		9.8	16.9	21.2	25.3	64.6	66.0

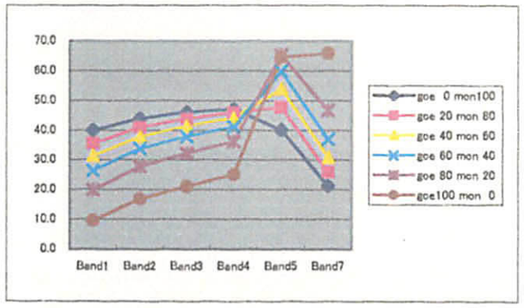

Mixed phase of goethite and montmorillonite									Band1	Band2	Band3	Band4	Band5	Band7
0	0	0	100	0	0	goe 0	mon100		40.1	44.1	46.2	47.2	40.3	21.5
0	0	20	80	0	0	goe 20	mon 80		35.7	41.1	44.1	46.1	47.9	26.2
0	0	40	60	0	0	goe 40	mon 60		31.5	38.0	41.5	44.3	54.0	31.0
0	0	60	40	0	0	goe 60	mon 40		26.6	33.9	38.1	41.5	60.0	37.1
0	0	80	20	0	0	goe 80	mon 20		20.1	27.9	32.4	36.4	65.3	46.7
0	0	100	0	0	0	goe100	mon 0		9.8	16.9	21.2	25.3	64.6	66.0

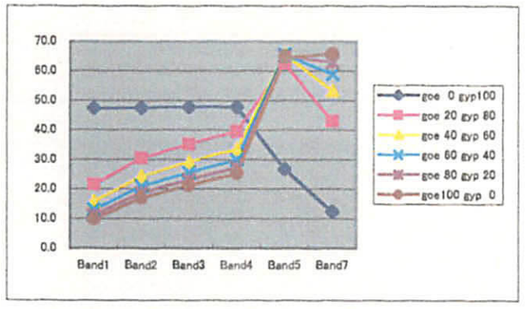

Mixed phase of goethite and gypsum									Band1	Band2	Band3	Band4	Band5	Band7
0	0	0	0	0	100	goe 0	gyp100		47.6	47.6	48.0	48.0	26.8	12.4
0	0	20	0	0	80	goe 20	gyp 80		21.7	30.5	35.4	39.8	62.5	43.1
0	0	40	0	0	60	goe 40	gyp 60		16.0	24.4	29.4	33.8	65.6	53.3
0	0	60	0	0	40	goe 60	gyp 40		13.1	21.1	25.8	30.1	65.7	59.1
0	0	80	0	0	20	goe 80	gyp 20		11.3	18.8	23.3	27.5	65.3	63.0
0	0	100	0	0	0	goe100	gyp 0		9.9	17.0	21.3	25.4	64.6	65.9

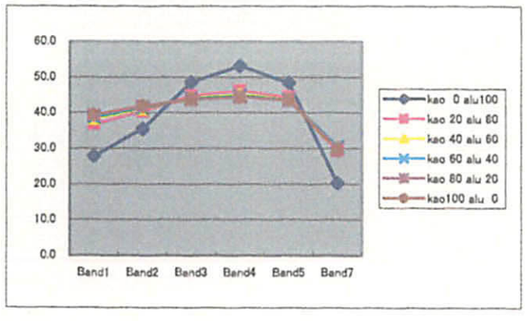

Mixed phase of kaoline and alunite									Band1	Band2	Band3	Band4	Band5	Band7
0	0	0	0	100	0	kao 0	alu100		28.0	35.6	48.6	53.2	48.5	20.3
0	0	0	20	80	0	kao 20	alu 80		36.9	40.4	44.9	46.4	44.6	29.4
0	0	0	40	60	0	kao 40	alu 60		38.3	41.1	44.2	45.2	43.9	30.3
0	0	0	60	40	0	kao 60	alu 40		39.0	41.5	43.9	44.7	43.7	30.5
0	0	0	80	20	0	kao 80	alu 20		39.3	41.8	43.7	44.5	43.6	30.2
0	0	0	100	0	0	kao100	alu 0		39.5	42.0	43.7	44.5	43.7	29.6

Fig. II-2-12 Spectral pattern of mixed phase of two minerals of Index 1 and Index 2

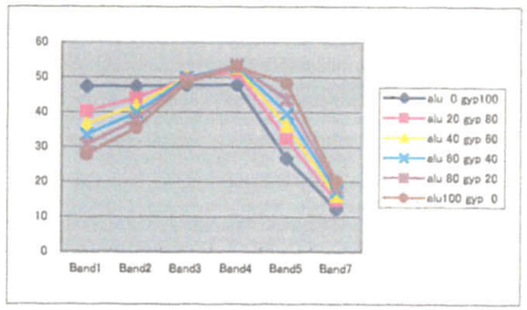

Mixed phase of alunite and gypsum

								Band1	Band2	Band3	Band4	Band5	Band7
0	0	0	0	0	100	alu 0	gyp100	47.6	47.6	48.0	48.0	26.8	12.4
0	0	0	0	20	80	alu 20	gyp 80	40.3	44.2	49.8	51.6	32.6	14.8
0	0	0	0	40	60	alu 40	gyp 60	36.8	42.1	50.2	52.8	36.3	16.2
0	0	0	0	60	40	alu 60	gyp 40	33.8	40.0	50.1	53.4	39.9	17.5
0	0	0	0	80	20	alu 80	gyp 20	30.9	38.0	49.6	53.6	43.8	18.8
0	0	0	0	100	0	alu100	gyp 0	28.0	35.6	48.6	53.2	48.5	20.3

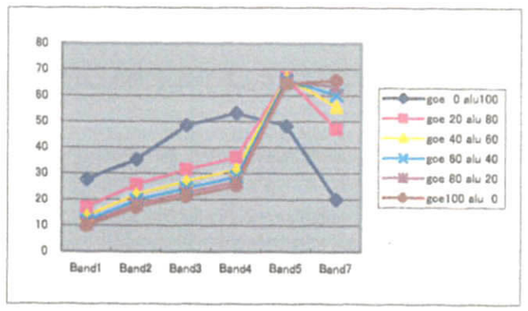

Mixed phase of goethite and alunite

								Band1	Band2	Band3	Band4	Band5	Band7
0	0	0	0	100	0	goe 0	alu100	28.0	35.6	48.6	53.2	48.5	20.3
0	0	20	0	80	0	goe 20	alu 80	17.2	25.8	31.8	36.3	66.9	47.3
0	0	40	0	60	0	goe 40	alu 60	13.8	22.0	27.2	31.6	66.9	55.8
0	0	60	0	40	0	goe 60	alu 40	12.0	19.8	24.6	28.9	66.1	60.4
0	0	80	0	20	0	goe 80	alu 20	10.8	18.3	22.8	27.0	65.3	63.5
0	0	100	0	0	0	goe100	alu 0	9.9	17.0	21.3	25.4	64.6	65.9

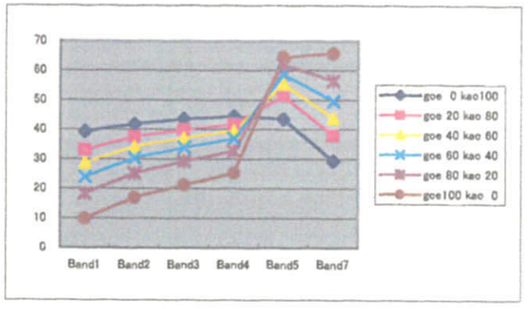

Mixed phase of goethite and kaoline

								Band1	Band2	Band3	Band4	Band5	Band7
0	0	0	100	0	0	goe 0	kao100	39.5	42.0	43.7	44.5	43.7	29.6
0	0	20	80	0	0	goe 20	kao 80	33.2	37.6	40.1	41.9	51.6	38.2
0	0	40	60	0	0	goe 40	kao 60	28.8	34.3	37.3	39.8	55.6	44.0
0	0	60	40	0	0	goe 60	kao 40	24.2	30.5	34.0	37.1	58.9	49.8
0	0	80	20	0	0	goe 80	kao 20	18.4	25.3	29.4	32.9	62.1	56.7
0	0	100	0	0	0	goe100	kao 0	9.9	17.0	21.3	25.4	64.6	65.9

Fig. II-2-12 (Continued)

	Band1	Band2	Band3	Band4	Band5	Band7
DN	72	34	45	33	79	34
Dnmin	40	10	5	1	−2	−4
coefficient	0.359	0.544	0.358	0.432	0.257	0.53
pseudo-reflectance	11.49	13.06	14.32	13.82	20.82	20.14

alteration mi	Q	Goe	Hem	Mon	Hal	Ser
ratio of mixt	0	50	10	0	0	40

	Band1	Band2	Band3	Band4	Band5	Band7
calculated reflectance	24.78	30.47	33.73	36.34	55.12	54.42

	Band1	Band2	Band3	Band4	Band5	Band7
cosine of psudo-reflectance	0.293	0.333	0.365	0.353	0.531	0.514
final result	0.248	0.305	0.337	0.363	0.551	0.544

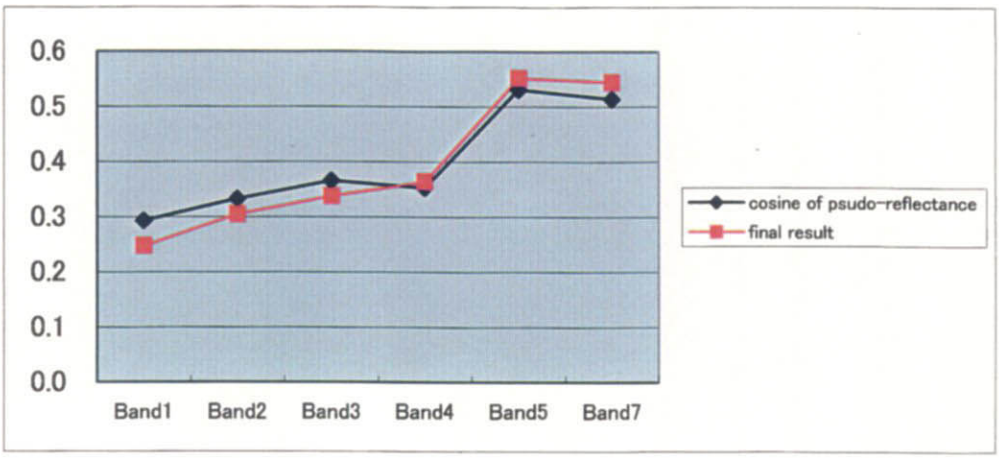

Result on referring the most fitted pseudo-reflectance of pixel to index 2

	Band1	Band2	Band3	Band4	Band5	Band7
DN	105	60	92	69	165	58
Dnmin	43	12	7	2	−1	−4
coefficient	0.325	0.544	0.357	0.430	0.305	0.640
pseudo-reflectance	20.15	26.112	30.345	28.81	50.63	39.68

alteration mi	Q	Goe	Hem	Kao	Alu	Gyp
ratio of mixt	20	20	0	0	60	0

	Band1	Band2	Band3	Band4	Band5	Band7
calculated reflectance	19.3	27.2	32.4	36.5	63.7	49.6

	Band1	Band2	Band3	Band4	Band5	Band7
cosine of psudo-reflectance	0.2412	0.3126	0.3633	0.3449	0.6062	0.4751
final result	0.1928	0.2724	0.324	0.3645	0.6365	0.4956

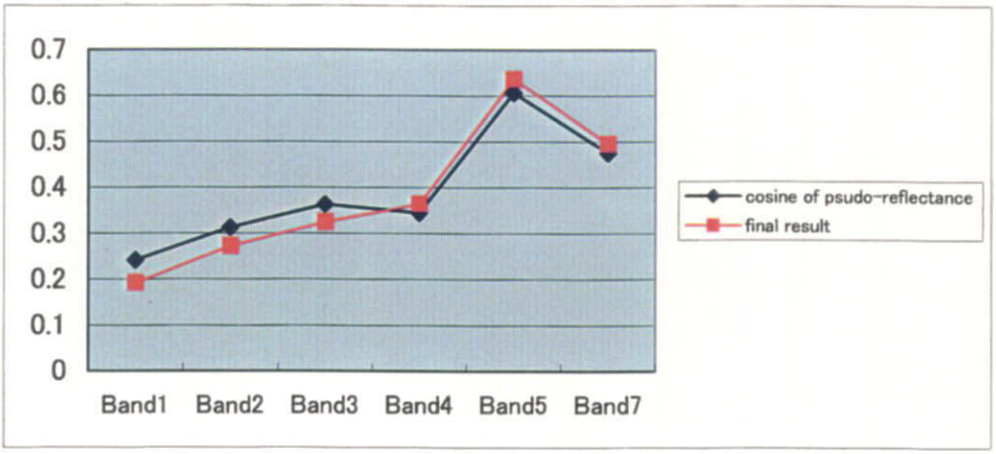

Fig. II-2-13 Examples of result on the pattern matching between reflectance of the iso-grain model and LANDSAT TM data

1) Malargue area (Fig. II-2-14a)

Although alteration zones[2)] have been extracted in the parts of alteration zones[1)] showing bright reddish purple on the ratio image, these have not been extracted in the slightly light reddish purple parts. On the other hand, several alteration zones[2)] have been extracted in the part that shows slightly dark reddish purple on the ratio image, and where alteration zones[1)] have not been extracted.

2) Chos Malal area (Fig. II-2-14b)

Regarding the three alteration zones[1)] in Cordillera de Los Andes zone in the west, alteration zones[2)] have been extracted in a limited part of this area.

Regarding the 12 alteration zones[1)] in Cordillera del Viento zone in the middle, alteration zones[2)] have been extracted within the area or at the very nearby places. Alteration zones[2)] also have been extracted in other places, and this tendency is prominent particularly on the southern side. Because almost all of them correspond to reddish purple areas on the ratio image, these zones are interpreted as alteration zones that could not be extracted in the first fiscal year (phase 1) survey.

Regarding the six alteration zones[1)] in the mountainous area to the northeast of Chos Malal in the east, although alteration zones[2)] have been extracted within this area or at very nearby places, the degree of consistency varies according to the places. Ring structure of 30 km in diameter is observed with CM020 as a center, and alteration zones[2)] have been sporadically extracted in them.

Regarding areas without alteration zones[1)] located in the central to eastern part, alteration zones[2)] are observed sporadically and widely in the southern part. The geological unit of this place was judged to be andesitic and basaltic volcanics of the Pliocene, but they are hardly interpreted as alteration zones from their occurrence behavior.

3) Zapla area (Fig. II-2-14c)

Alteration zones[1)] with the NNW-SSE oriented trend have been extracted in a relatively narrow scope from the central part to the eastern part of this area. A distinctive feature of these zones is a close relationship with places with high density of extracted lineaments. Alteration zones[2)] as a whole have been extracted in almost the same scope as alteration zones[1)] and also have the NNW-SSE oriented trend. When each of these zones is seen as an independent alteration zone, however, they do not show very good consistency. In places where alteration zones[1)] have not been extracted, alteration zones[2)] have been extracted in the area where Jurassic sedimentary rocks occur.

4) San Carlos de Bariloche area (Fig. II-2-14d)

Many alteration zones[1)] of small scale have been extracted in the zone in the south-to-north direction in the central to eastern part of this area. Though the consistency of alteration zones[1)] and alteration zones[2)] is not very good, almost all alteration zones[2)] have been extracted near alteration zones[1)]. This is considered to show the limit of accuracy in visually extracting alteration zones from the ratio image. As a distinctive feature of this area, the distribution of both alteration zones[1)] and [2)] are limited.

5) Lago Menendes area (Fig. II-2-14e)

Two-thirds of a scene of the image on the western side belongs to the Republic of Chile, and one-third of the scene represents the area. Alteration zones[1)] have been extracted in the zone in the north-south direction near the eastern edge of this area. Alteration zones[2)] have been extracted at almost the same locations as alteration zones[1)]. But places also are observed where alteration zones[2)] have not been extracted while alteration zones[1)] have been extracted. As a result of re-checking the ratio image it is considered that these alteration zones[1)] have been extracted by mistake. There are no places where only alteration zones[2)] have been extracted.

6) Esuquel area (Fig. II-2-14f)

Regarding alteration zones[1)] extracted as a zone with the two trends of the north-south direction on the west side of this area, alteration zones[2)] have been extracted within the area or in its vicinity. Although this is consistent with alteration zones[1)] as a zone with the trend of the N-S direction, there are many cases where alteration zones[2)] have been extracted where alteration zones[1)] have not been extracted.

On the eastern side of this area, alteration zones[1)] have been sporadically extracted in six places only, and alteration zones[2)] are slightly and narrowly distributed in these bounds. Alteration zones[2)] mainly with Index 1 show distribution of a wide area in the district without alteration zones[1)]. These correspond to areas where sedimentary rocks of the Jurassic to Cretaceous and volcanics of the Tertiary occur, and these extracts may not represent actual alteration zones.

Correspondence to the result of field survey is described in "Chapter 3. Ground truth." In the stage where comparison with alteration zones extracted in the first fiscal year (phase 1) survey have been made on the maps, the results of analysis of this fiscal year (phase 2) is summarized as follows:

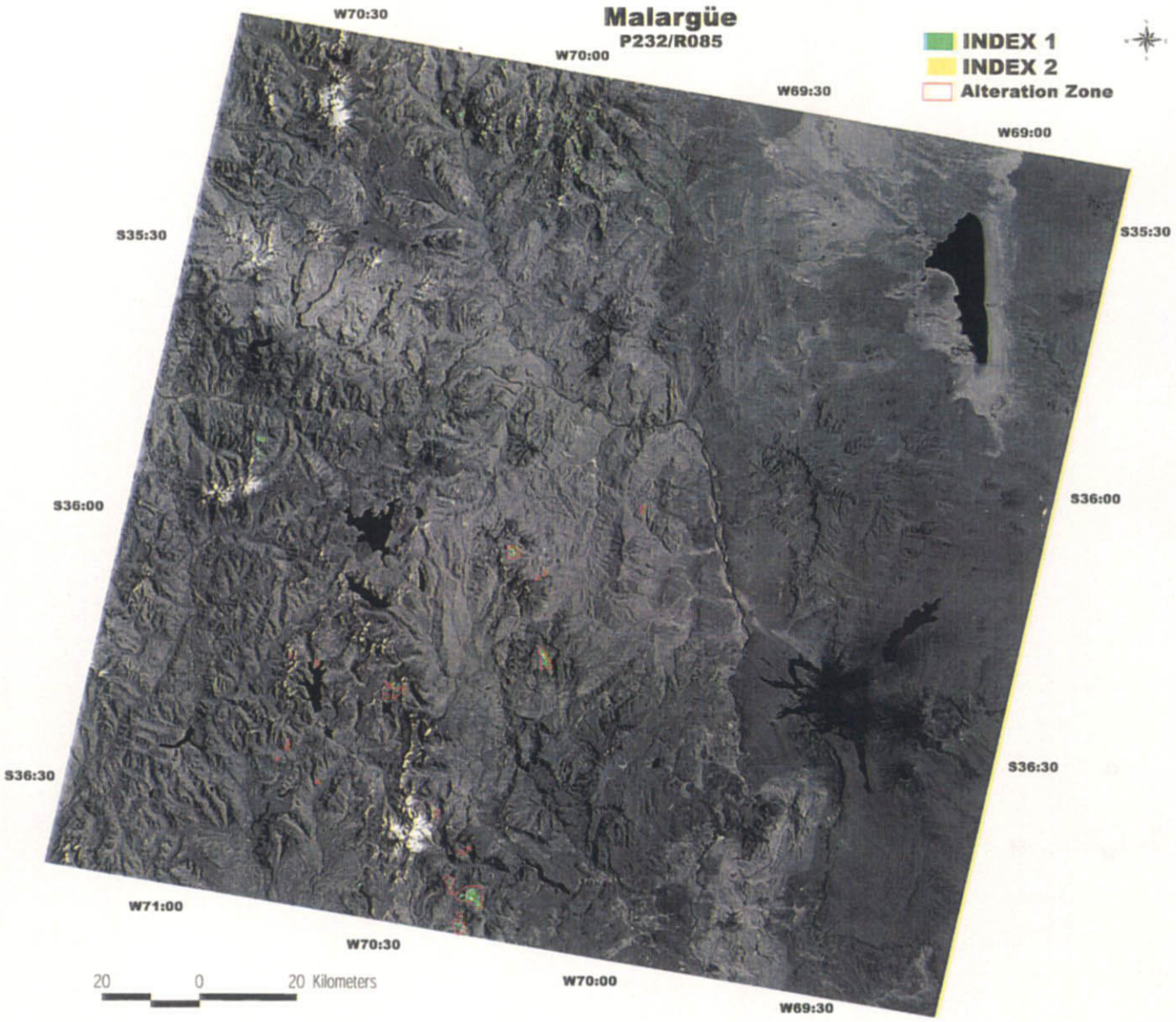

Fig. II-2-14a LANDSAT TM image of the Malargue area displaying alteration zones of Index 1 (green) and Index 2 (yellow)

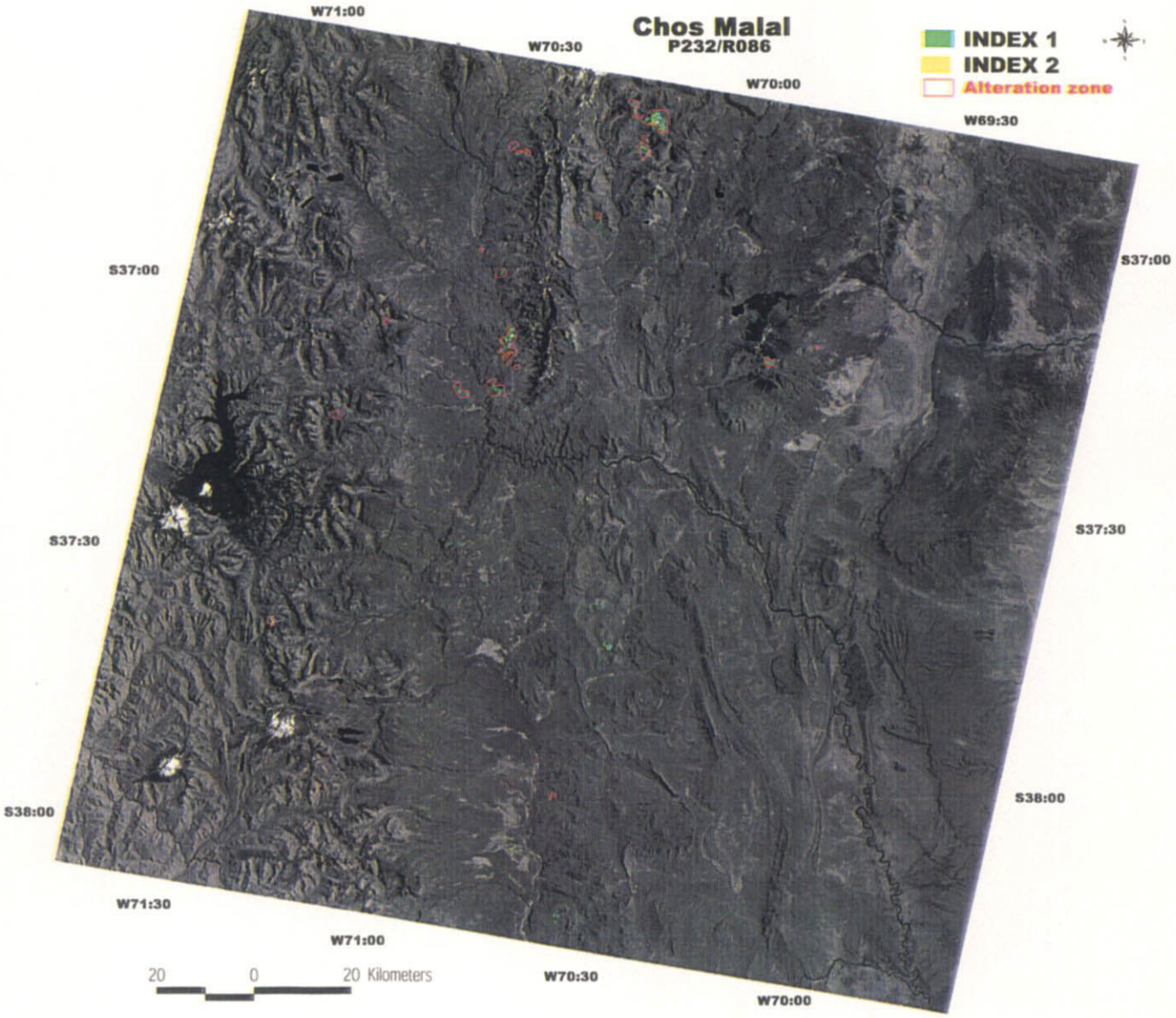

Fig. II-2-14b LANDSAT TM image of the Chos Malal area displaying alteration zones of Index 1 (green) and Index 2 (yellow)

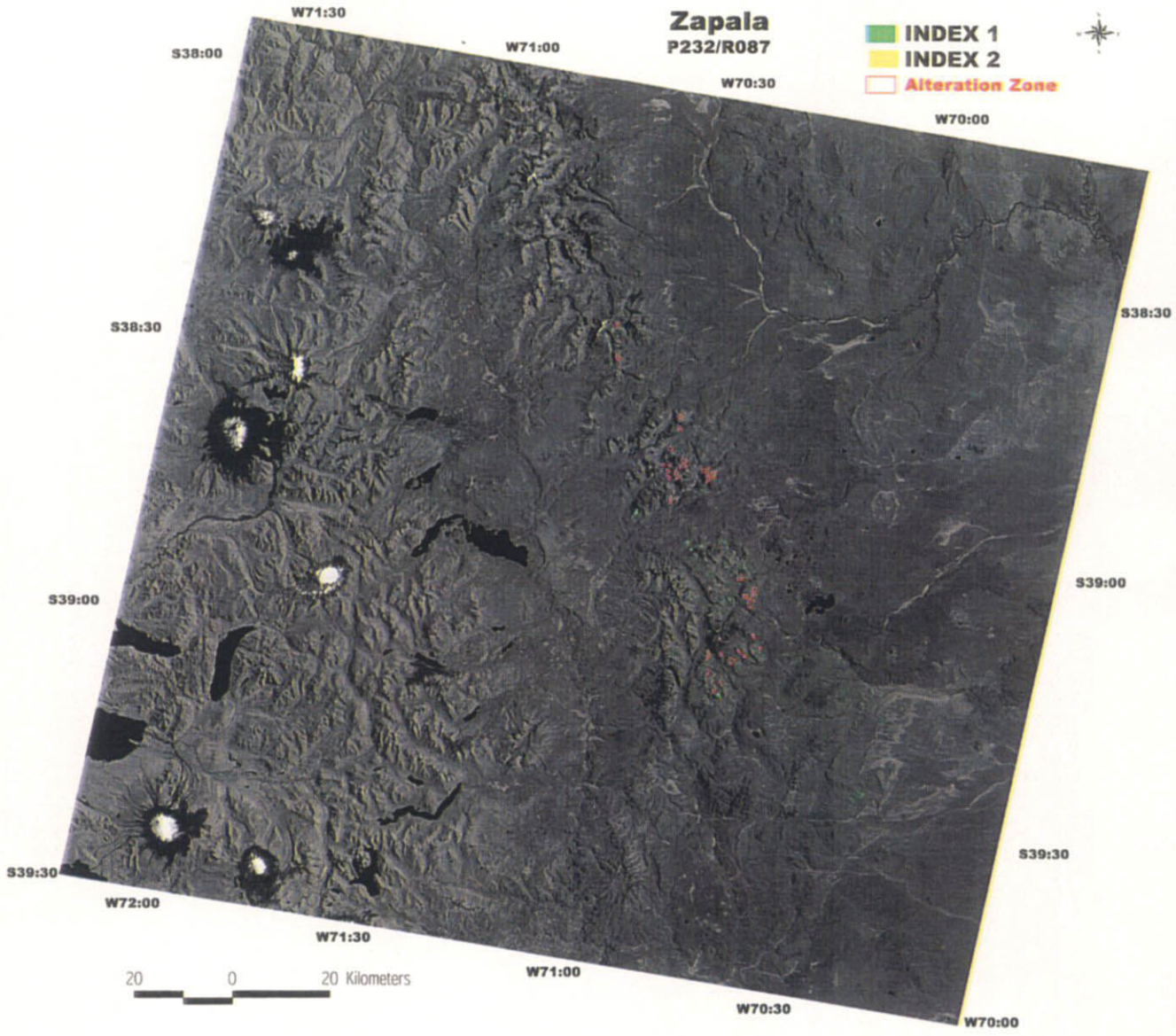

Fig. II-2-14c LANDSAT TM image of the Zapala area displaying alteration zones of Index 1 (green) and Index 2 (yellow)

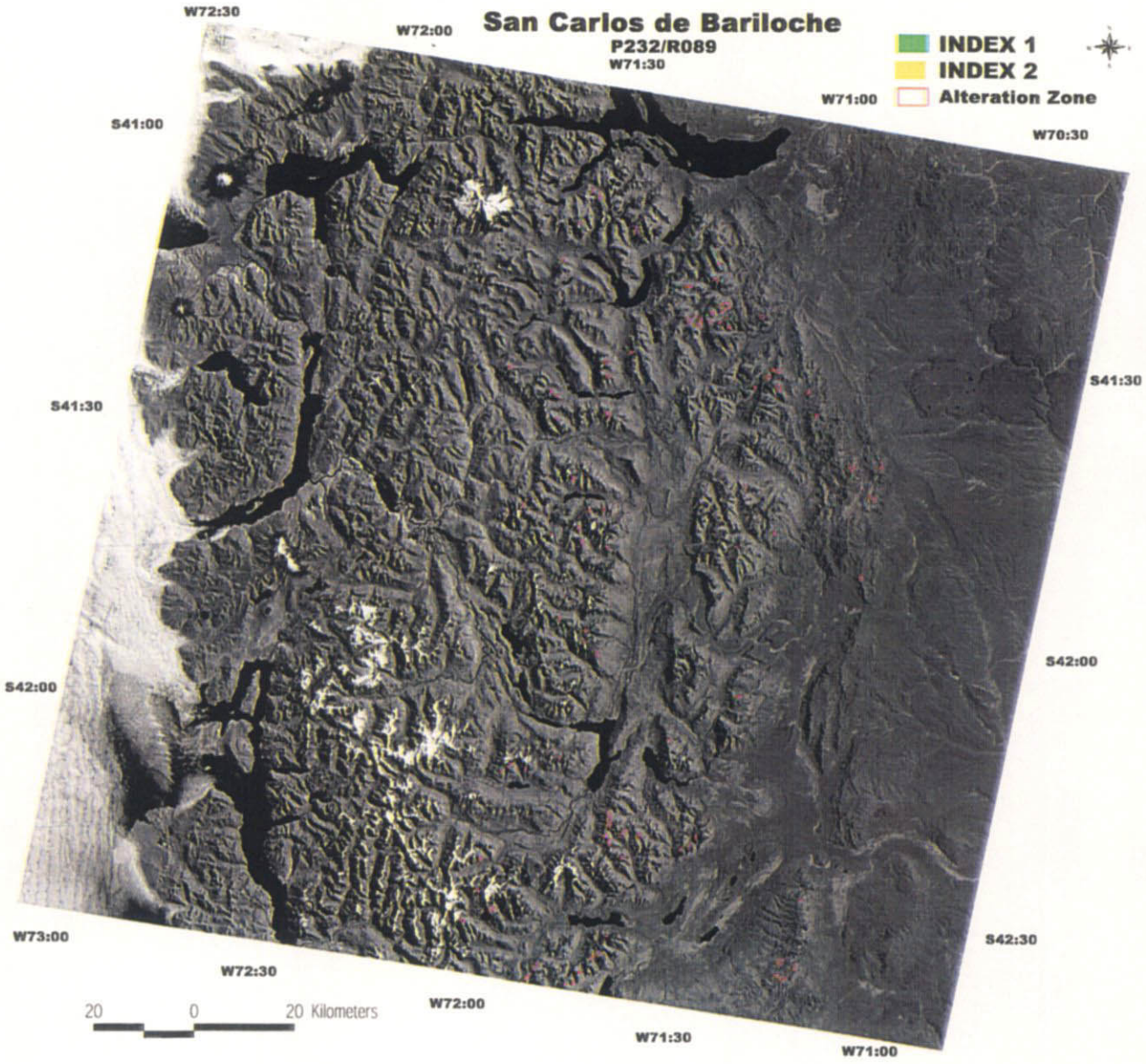

Fig. II-2-14d LANDSAT TM image of the San Carlos de Bariloche area displaying alteration zones of Index 1 (green) and Index 2 (yellow)

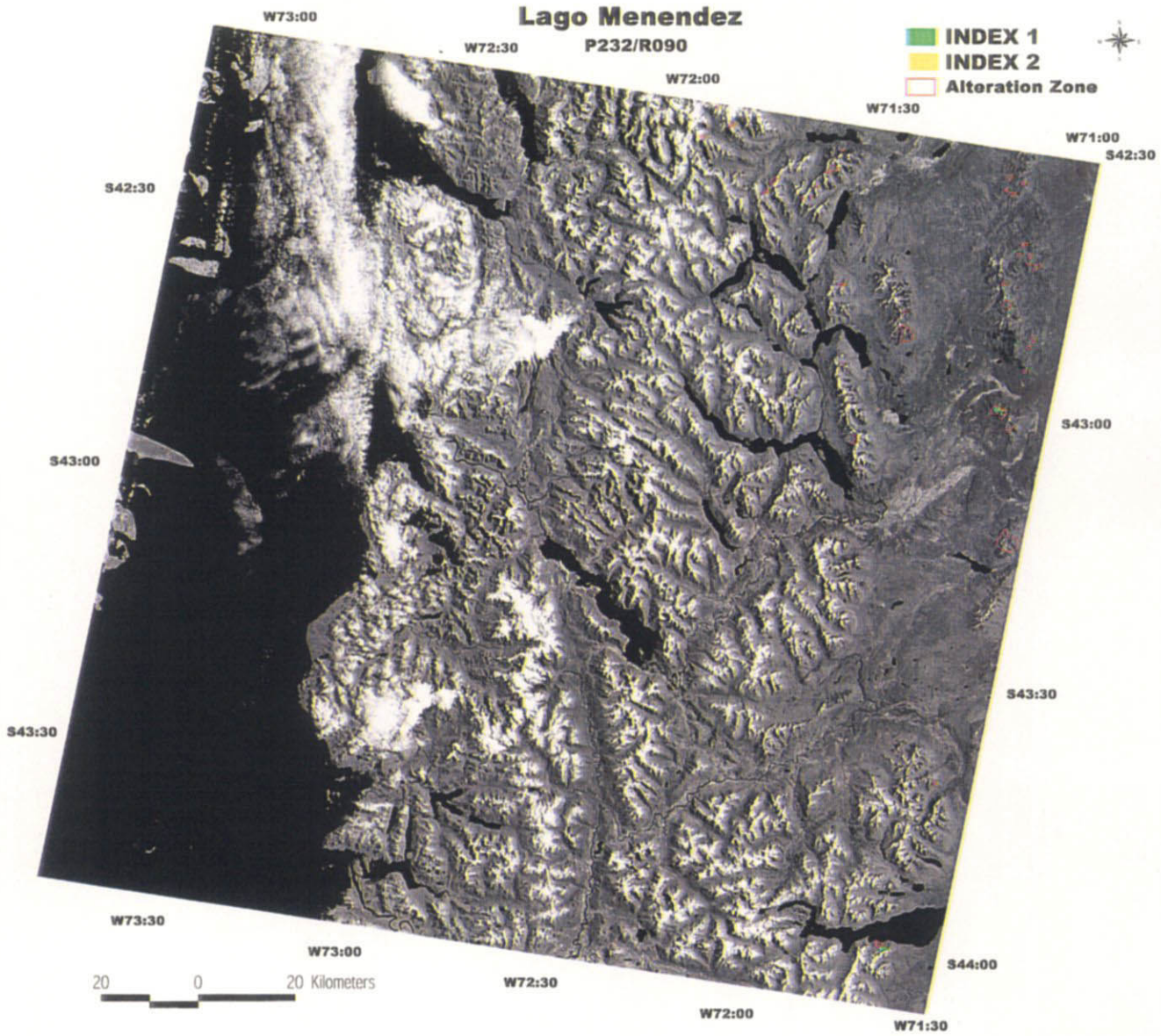

Fig. II-2-14e LANDSAT TM image of the Lago Menendez area displaying alteration zones of Index 1 (green) and Index 2 (yellow)

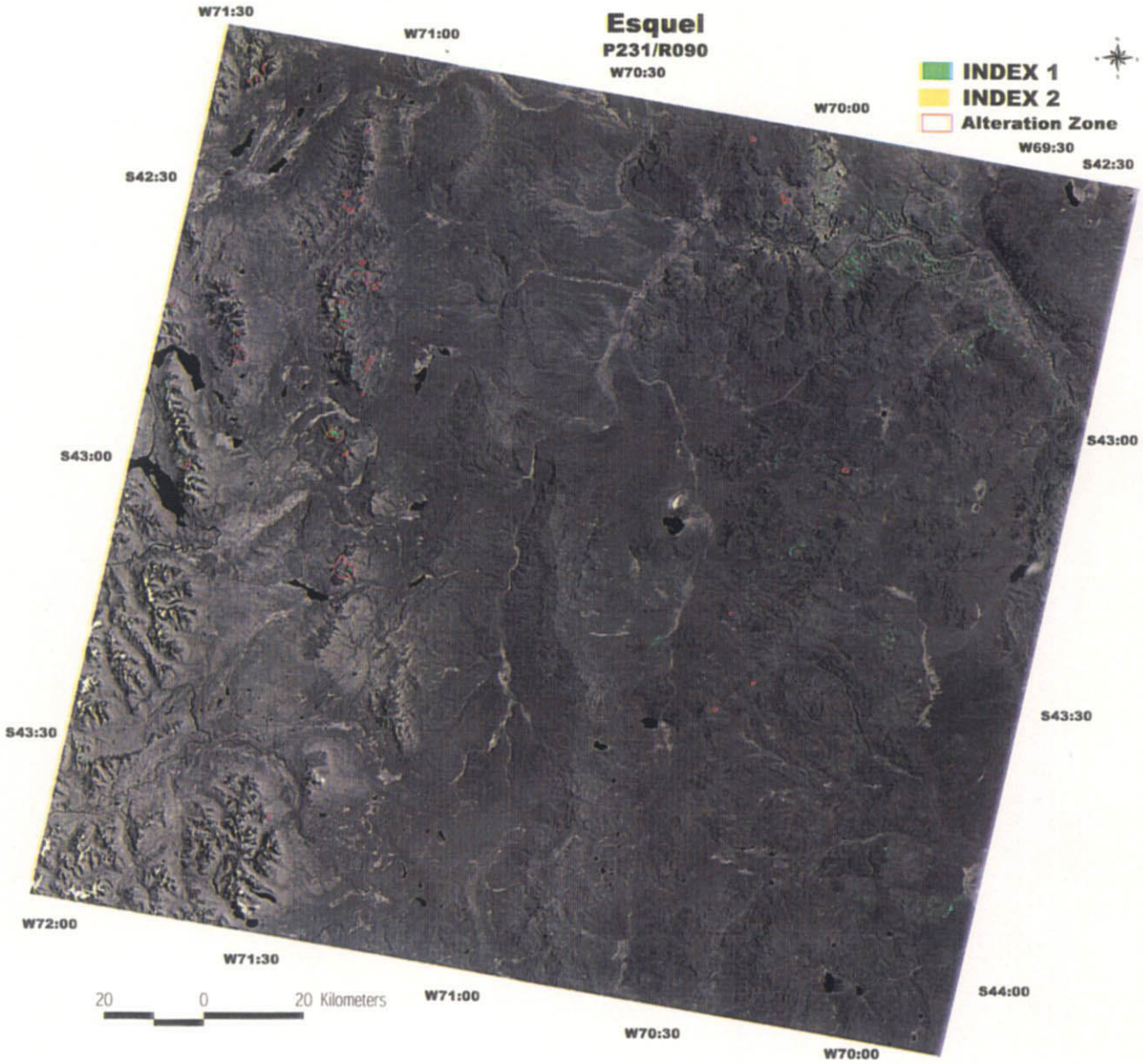

Fig. II-2-14f LANDSAT TM image of the Esquel area displaying alteration zones of Index 1 (green) and Index 2 (yellow)

* Concerning areas where hydrothermal alteration zones are distributed, it is judged that precise analysis of alteration zones extracts hydrothermal alteration zones at higher accuracy. This is considered to result mainly from the limitation in accuracy of visual extraction on the ratio image.

* It is desirable that results of this analytical method should be examined and interpreted after geological units and structures are interpreted first with reference to the false color image and the ratio image.